

ELECTROMAGNETIC SCATTERING ANALYSIS AND DESIGN OF  
SANDWICH TYPE RADOMES

A THESIS SUBMITTED TO  
THE GRADUATE SCHOOL OF NATURAL AND APPLIED SCIENCES  
OF  
MIDDLE EAST TECHNICAL UNIVERSITY

BY

MEHMET MURAT ŞEREFOĞLU

IN PARTIAL FULLFILLMENT OF THE REQUIREMENTS  
FOR  
THE DEGREE OF MASTER OF SCIENCE  
IN  
ELECTRICAL AND ELECTRONICS ENGINEERING

APRIL 2009

Approval of the thesis:

**ELECTROMAGNETIC SCATTERING ANALYSIS AND DESIGN OF  
SANDWICH TYPE RADOMES**

submitted by **MEHMET MURAT ŞEREFOĞLU** in partial fulfillment of the  
requirements for the degree of **Master of Science in Electrical and  
Electronics Engineering Department, Middle East Technical University**  
by,

Prof. Dr. Canan Özgen

Dean, Graduate School of **Natural and Applied Sciences**

Prof. Dr. İsmet Erkmén

Head of Department, **Electrical and Electronics Engineering**

Prof. Dr. Gülbin Dural

Supervisor, **Electrical and Electronics Engineering Dept., METU**

**Examining Committee Members:**

Prof. Dr. Altunkan Hızal

Electrical and Electronics Engineering Dept., METU

Prof. Dr. Gülbin Dural

Electrical and Electronics Engineering Dept., METU

Prof. Dr. Nilgün Günalp

Electrical and Electronics Engineering Dept., METU

Prof. Dr. Canan Toker

Electrical and Electronics Engineering Dept., METU

Celal Dudak

Msc, TÜBİTAK

**Date:**

**I hereby declare that all information in this document has been obtained and presented in accordance with academic rules and ethical conduct. I also declare that, as required by these rules and conduct, I have fully cited and referenced all material and results that are not original to this work.**

Name, Last name : Mehmet Murat ŞEREFOĞLU

Signature :

## **ABSTRACT**

# **ELECTROMAGNETIC SCATTERING ANALYSIS AND DESIGN OF SANDWICH TYPE RADOMES**

Şerefoğlu, Mehmet Murat

M. Sc., Department of Electrical and Electronics Engineering

Supervisor: Prof. Dr. Gülbin Dural

April 2009, 103 pages

In this thesis work, importance of radome structures for antenna systems is emphasized. Structural and electromagnetic requirements of various types of radome structures are analyzed and specific properties are given. Electromagnetic scattering analysis of sandwich type radome seams has been done. Total antenna system far electromagnetic field expression, which is the combination of original antenna far electromagnetic field and the scattered electromagnetic field of the framework of the sandwich radome structure has been found and simulated. To enhance electromagnetic transparency of sandwich type radomes two sandwich radome design methods are proposed which are expressed as Geometrical Randomization and Tuning the Seams. Electromagnetic scattering level minimizations advanced by these design methods are presented with related simulations.

Keywords: Scattering Analysis of Sandwich Radomes, Tuning the Seams,  
Geometric Randomization, Quasi-Random Designed Radome Geometry,

# ÖZ

## SANDVIÇ TİPİ ANTEN KAPORTALARININ ELEKTROMANYETİK SAÇILIM ANALİZİ VE TASARIMI

Şerefoğlu, Mehmet Murat

Yüksek Lisans, Elektrik-Elektronik Mühendisliği Bölümü

Tez Yöneticisi: Prof. Dr. Gülbin Dural

Nisan 2009, 103 sayfa

Bu tez çalışmasında anten kaportası yapılarının anten sistemleri için önemine vurgu yapılmıştır. Çeşitli anten kaportalarının yapısal ve elektromanyetik gereksinimleri analiz edilerek spesifik özellikleri verilmiştir. Sandviç tipi anten kaportalarının elektromanyetik saçılım analizi yapılmıştır. Orijinal anten uzak elektromanyetik dalgasının ve sandviç anten kaportası iskeletinden saçılan elektromanyetik dalganın kombinasyonundan oluşan toplam anten sistemi uzak elektromanyetik dalgası bulunarak benzetimi yapılmıştır. Sandviç anten kaportalarının elektromanyetik geçirgenliğini artırabilmek için Geometrik Rastlantısallık ve Eklem Yeri Dalga Ayarlama şeklinde ifade edilen iki tasarım yöntemi önerilmiştir. Bu tasarım yöntemleriyle kazanılan elektromanyetik saçılım seviyesindeki azalma ilgili benzetimlerle sunulmuştur.

Anahtar Kelimeler: Sandviç Anten Kaportalarının Saçılım Analizi, Eklem Yerlerinin Dalga Uyumu, Geometrik Rasgele Dağılım, Rasgele Tasarlanmış Anten Kaportası Geometrisi

To My Dear Family



## **ACKNOWLEDGEMENTS**

I would like to express my deepest gratitude to my supervisor Prof. Dr. Gülbin Dural for her encouragements, guidance, advice, criticism and insight throughout my thesis work.

I would like to thank to Prof. Dr. Altunkan HIZAL for his encouragement and guidance about my thesis work.

I would also like to express my profound appreciation to my dear family for their continuous support, motivation and patience throughout this thesis work as always in my life.

I would like to thank ASELSAN Inc. for their continuous support during my graduate study.

I would also like to thank Turkish Scientific and Technological Research Council (TÜBİTAK) for their financial assistance during my graduate study.

I would like to forward my appreciation to all my friends and colleagues who contributed to my thesis work with their continuous encouragement.

# TABLE OF CONTENTS

<b>ABSTRACT .....</b>	<b>iv</b>
<b>ÖZ.....</b>	<b>vi</b>
<b>ACKNOWLEDGEMENTS.....</b>	<b>ix</b>
<b>TABLE OF CONTENTS.....</b>	<b>x</b>
<b>LIST OF TABLES .....</b>	<b>xii</b>
<b>LIST OF FIGURES .....</b>	<b>xiii</b>
<b>LIST OF ABBREVIATIONS .....</b>	<b>xvii</b>
<b>CHAPTERS</b>	
<b>1. INTRODUCTION.....</b>	<b>1</b>
<b>2. RADOMES .....</b>	<b>4</b>
2.1 General Information .....	4
2.2 Necessity of Radomes .....	5
2.3 Requirements of Radomes .....	6
2.3.1 Mechanical Requirements of Radomes .....	7
2.3.2 Electromagnetic Requirements of Radomes .....	9
2.4 Radome Types.....	17
2.4.1 Solid Laminate Radomes .....	17
2.4.2 Dielectric Space Frame Radomes .....	19
2.4.3 Metal Space Frame Radomes .....	20
2.4.4 Air Pressurised Radomes .....	25
2.5 Sandwich Type Radomes .....	27
2.5.1 Features of Sandwich Type Radomes .....	28

2.5.2 Advantages of Sandwich Type Radomes.....	31
2.5.3 Disadvantages of Sandwich Type Radomes .....	32
2.5.4 Importance of Framework Structures in Sandwich Type Radomes .....	32
2.5.5 Structural and Electromagnetic Comparison of Different Sandwich Radome Framework Geometries .....	33
<b>3. ELECTROMAGNETIC SCATTERING ANALYSIS OF SEAMS IN SANDWICH TYPE RADOMES .....</b>	<b>37</b>
3.1 General Information .....	37
3.2 Scattering Analysis of Radome Seams .....	38
3.3 Total Far Field Expression of Antenna and Arbitrary Distributed Sandwich Radome Seams .....	46
3.4 Simulations Based on the Analysis .....	56
<b>4. ENHANCING ELECTROMAGNETIC TRANSPARENCY OF SANDWICH TYPE RADOMES .....</b>	<b>73</b>
4.1 Factors Effecting Electromagnetic Performance of the Structure...	73
4.2 Importance of the Distance of the Seam Structure to the Antenna Aperture .....	74
4.3 Enhancing Electromagnetic Transparency by Quasi-Random Geometric Distribution of Seams .....	79
4.4 Electromagnetic Transparency Enhancement by Tuning the Seams in Sandwich Type Radomes .....	86
4.4.1 Tuning the Seams in Sandwich Type Radomes .....	86
4.4.2 Effect of Tuning the Seams in Sandwich Type Radomes .....	87
<b>5. CONCLUSIONS .....</b>	<b>94</b>
<b>REFERENCES.....</b>	<b>98</b>
<b>APPENDIX .....</b>	<b>101</b>

## **LIST OF TABLES**

Table 1- Structural Comparison of Metal Space Frame Radomes and Dielectric Space Frame Radomes [2].....	24
Table 2- Structural Comparison of Quasi Random Sandwich Radome Geometry and Orange-Peel Sandwich Radome Geometry .....	36

## LIST OF FIGURES

Figure 1- Preparation of a radome panel for transportation [5] .....	8
Figure 2-Beginning, intermediate and final installation of a radome structure [6] .....	9
Figure 3 - Induced Field Ratio [9].....	11
Figure 4- Evaluating Hydrophobicity by Measuring the Contact Angle of the Water Droplet on the Surface [10] .....	14
Figure 5- Hydrophobic and Non-Hydrophobic Material Responses to Water .	15
Figure 6- Effect of Hydrophobic Coating on Transmission Loss [10] .....	16
Figure 7 - Solid Laminate Radome for Shipboard Data Communications [3] .	17
Figure 8 - 3.05 m Diameter Solid Laminate Radome for MK-86 Gun Fire Control System [3] .....	18
Figure 9 - Dielectric Space Frame Radome [2] .....	19
Figure 10- 14.1 m Diameter Metal Space Frame Radome [3].....	21
Figure 11- Beginning, Intermediate and Final Installations of Air Pressurised Radome [11] .....	26
Figure 12 -Sandwich Type Radome with Large Access Doors [3] .....	27
Figure 13- Sandwich Radome Types [13] .....	28
Figure 14- 3D Glass Material Used in Core Part of Type-A Sandwich Radomes [19] .....	29
Figure 15- Honeycomb Core Materials Used in Type-A Sandwich Radomes [19] .....	30
Figure 16- Sandwich Radome Panels and Framework Geometry .....	31
Figure 17- Typical Quasi Random Sandwich Radome Geometry.....	34
Figure 18 – Typical Orange Peel Sandwich Radome Geometry .....	34
Figure 19 - Scattering Geometry of the Analysis.....	40

Figure 20- Far E-Field Characteristics of Antenna and Different Sandwich Radome Seam Distributions .....	58
Figure 21- Design of Pyramidal Horn Antenna .....	59
Figure 22 – 3D Polar Plot of the Horn Antenna E-Field Pattern .....	60
Figure 23 - 3D Rectangular Plot of the Antenna E-Field Pattern .....	61
Figure 24- 2D Total E-Field Radiation Characteristics of the Antenna on Principal Planes .....	61
Figure 25- Placement of $4,8 \lambda$ Length and $0,2 \lambda$ Diameter Horizontal Sandwich Radome Seam at $6\lambda$ Distance to the Horn Antenna.....	63
Figure 26 - 3D Polar Plot of the Total E-Field Pattern of the $4,8 \lambda$ Length and $0,2 \lambda$ Diameter Horizontal Sandwich Radome Seam Placed at $6\lambda$ Distance to the Antenna .....	64
Figure 27 - 3D Rectangular Plot E-Field Pattern of the $4,8 \lambda$ Length and $0,2 \lambda$ Diameter Horizontal Sandwich Radome Seam Placed at $6\lambda$ Distance to the Antenna .....	65
Figure 28 - 2D Total E-Field Radiation Characteristics of $4,8 \lambda$ Length and $0,2 \lambda$ Diameter Horizontal Sandwich Radome Seam Placed at $6\lambda$ Distance to the Antenna .....	65
Figure 29- Placement of $4,8 \lambda$ Length and $0,2 \lambda$ Diameter Perpendicular Sandwich Radome Seam at $6\lambda$ Distance to the Antenna.....	66
Figure 30 - 3D Polar Plot of the E-Field Pattern with $4,8 \lambda$ Length and $0,2 \lambda$ Diameter Perpendicular Sandwich Radome Seam in the Near Field of the Antenna .....	67
Figure 31 - 3D Rectangular Plot of the E-Field Pattern of the $4,8 \lambda$ Length and $0,2 \lambda$ Diameter Perpendicular Sandwich Radome Seam and the Antenna .....	68
Figure 32- 2D Total E-Field Radiation Characteristics of $4,8 \lambda$ Length and $0,2 \lambda$ Diameter Perpendicular Sandwich Radome Seam Placed at $6\lambda$ Distance to the Antenna .....	68
Figure 33- Multi Numbered Distribution of $4,8 \lambda$ Length and $0,2 \lambda$ Diameter Sandwich Radome Seams Placed at $6\lambda$ Distance to the Antenna.....	70

Figure 34 - 3D Polar Plot of the E-Field of the Distributed $4,8 \lambda$ Length and $0,2 \lambda$ Diameter Sandwich Radome Seams Placed at $6\lambda$ Distance to the Antenna .....	71
Figure 35 - 2D Total E-Field Radiation Characteristics of Distributed $4,8 \lambda$ Length and $0,2 \lambda$ Diameter Sandwich Radome Seams Placed at $6\lambda$ Distance to the Antenna.....	71
Figure 36 - $4,8 \lambda$ Length and $0,2 \lambda$ Diameter Sandwich Radome Seam Placed at $3 \lambda$ Distance to the Aperture .....	75
Figure 37 - $4,8 \lambda$ Length and $0,2 \lambda$ Diameter Sandwich Radome Seam Placed at $10.7\lambda$ Distance to the Aperture.....	75
Figure 38 - 3D Cartesian Plot of the Total E-Field Pattern of $3\lambda$ Distant $4,8 \lambda$ Length and $0,2 \lambda$ Diameter Sandwich Radome Seam .....	77
Figure 39 - 3D Cartesian Plot of the Total E-Field Pattern of $10.7\lambda$ Distant $4,8 \lambda$ Length and $0,2 \lambda$ Diameter Sandwich Radome Seam.....	77
Figure 40 - Polar Plot of the Total E-Field Pattern of $3\lambda$ Distant $4,8 \lambda$ Length and $0,2 \lambda$ Diameter Sandwich Radome Seam.....	78
Figure 41 - Polar Plot of the Total E-Field Pattern of $10.7\lambda$ Distant $4,8 \lambda$ Length and $0,2 \lambda$ Diameter Sandwich Radome Seam .....	78
Figure 42 – 18.9 Meter Diameter Sandwich Radome Panels and Panel Framework Geometry [3].....	80
Figure 43 – Orange-Peel Radome Framework Design with $2,8 \lambda$ Length and $0,2 \lambda$ Diameter 12 Seams Placed at $6\lambda$ Distance to the Antenna .....	81
Figure 44 - 3D Polar Plot of Total E-Field Pattern of Orange-Peel Type Designed Sandwich Radome Framework with $2,8 \lambda$ Length and $0,2 \lambda$ Diameter 12 Seams Placed at $6\lambda$ Distance to the Antenna.....	82
Figure 45 - 3D Rectangular Plot of the E-Field Pattern Characteristics of Orange-Peel Type Designed Sandwich Radome Framework with $2,8 \lambda$ Length and $0,2 \lambda$ Diameter 12 Seams Placed at $6\lambda$ to the Antenna .....	83
Figure 46 – Randomized Distribution of $2,8 \lambda$ Length and $0,2 \lambda$ Diameter 12 Seams Placed at Approximately $6\lambda$ Distance In Front of the Antenna .....	84

Figure 47 - 3D Polar E-Field Pattern of Random Distributed $2,8 \lambda$ Length and $0,2 \lambda$ Diameter 12 Seams Placed at Approximately $6\lambda$ Distance In Front of the Antenna.....	85
Figure 48- 3D Rectangular Total E-Field Pattern of Random Distributed $2,8 \lambda$ Length and $0,2 \lambda$ Diameter 12 Seams Placed at Approximately $6\lambda$ Distance In Front of the Antenna .....	85
Figure 49 – Horizontal Silicon Dioxide Cylinder Seam with $4,8 \lambda$ Length and $0,47 \lambda$ Diameter Placed at $5 \lambda$ Distance to the Horn Antenna .....	88
Figure 50 - 3D Polar Total E-Field of the Horizontal Silicon Dioxide Seam with $4,8 \lambda$ Length and $0,47 \lambda$ Diameter Placed at $5 \lambda$ Distance to the Horn Antenna .....	88
Figure 51 - 3D Rectangular Total E-Field of the Horizontal Silicon Dioxide Seam with $4,8 \lambda$ Length and $0,47 \lambda$ Diameter Placed at $5 \lambda$ Distance to the Horn Antenna .....	89
Figure 52 - 2D Total E-Field of the Horizontal Silicon Dioxide Seam with $4,8 \lambda$ Length and $0,47 \lambda$ Diameter Placed at $5 \lambda$ Distance to the Horn Antenna .....	89
Figure 53 - Tuning Mechanism of the Silicon Dioxide Dielectric Seam with Perfect Electric Conductors.....	91
Figure 54 -3D Polar Plot of the Total E-Field Pattern of the Tuned Seam with $4,8 \lambda$ Length and $0,47 \lambda$ Diameter Placed at $5 \lambda$ Distance to the Horn Antenna .....	92
Figure 55 - 3D Rectangular Plot of the E-Field Pattern of the Tuned Seam with $4,8 \lambda$ Length and $0,47 \lambda$ Diameter Placed at $5 \lambda$ Distance to the Horn Antenna .....	92
Figure 56 - 2D Total E-Field Radiation Characteristics of Tuned Sandwich Radome Seam with $4,8 \lambda$ Length and $0,47 \lambda$ Diameter Placed at $5 \lambda$ Distance to the Horn Antenna .....	93



## **LIST OF ABBREVIATIONS**

DSF	: Dielectric Space Frame
FRP	: Fiberglass Reinforced Plastic
MSF	: Metal Space Frame
SLR	: Solid Laminate Radome
SRS	: Sandwich Radome Seam
TE	: Transverse Electric
TM	: Transverse Magnetic
VSWR	: Voltage Standing Wave Ratio

# **CHAPTER 1**

## **INTRODUCTION**

Typically, large antenna systems are covered with radomes in order to protect them from harsh weather conditions and to enable them to operate continuously without loss of precision. Radomes enhance performance of operation of the antenna systems in harsh atmospheric conditions such as intense wind, sand, rain, corrosion etc. They are also very crucial for decreasing life time cost of large antenna systems. There are various types of radome structures for specific purposes of the antenna systems. Depending on the size of the antennas the radomes are usually assembled from many panels which are connected together forming joints or seams. In high performance discrete narrow bandwidth applications, the panels are usually Type-A sandwiches that are optimized for minimum transmission loss over moderately narrow bandwidths. However, the physical dimensions of the panel framework, in other words, radome seams are usually determined by structural considerations, such as maximum wind speed or other resultant stresses they have to sustain. However, without electromagnetic consideration, the framework degrades the total system performance by introducing high scattering levels. Therefore, it is very crucial for the whole system to minimize this scattering effect due to the framework while protecting the antenna system.

In this thesis work, requirements of radomes are expressed. Various types of radome structures and their specific properties are presented. Detailed information about Sandwich Radomes is expressed. Electromagnetic scattering analysis of sandwich type radomes is done. To enhance electromagnetic transparency of radome seams in the sandwich radomes, two different design methods are proposed which are named as Geometrical Randomization and Tuning the Seams.

In Chapter 2, general information about radomes including definition, the purpose of usage and necessity is given. Mechanical and electromagnetic requirements of radomes are investigated. Factors affecting the electromagnetic performance of radomes such as insertion loss and scattering loss are defined. Importance of Hydrophobic coating on the outermost side of the radome panel structure is emphasized. Information about different radome types including antenna systems they cover, the operational frequency band, general size of the structures and cost information is given. Detailed information including advantages and disadvantages of Sandwich Radomes is expressed. Electromagnetic importance of the framework geometry in Sandwich Radomes is investigated. Finally, structural and electromagnetic properties of two common Sandwich Radome geometries are discussed.

Chapter 3 is devoted to electromagnetic scattering analysis of Sandwich Radomes. The analysis is applicable to all type of antennas with the condition of knowledge of near and far electromagnetic field equations of the antenna inside. Pyramidal horn type of antenna is used as a case study for the analysis. Scattering by arbitrarily distributed radome seams is formulated. Total far electromagnetic fields including antenna far electromagnetic fields and scattering electromagnetic fields from arbitrarily

distributed radome seams are formulated. Simulations based on the analysis are performed and the effect of scattering is visualized.

In Chapter 4, the ways of enhancing electromagnetic transparency of the Sandwich Radome Seams (SRS) are investigated. Two different design methods are proposed to enhance transparency. They are named as Geometrical Randomization and Tuning the Seams. Both methods are expressed in detail, and the effect of transparency enhancement by the methods is visualized by related simulations.

Chapter 5 is devoted to the conclusion of this thesis work. This chapter summarizes all the work done in this thesis work. Finally, possible future work areas about sandwich radomes are mentioned considering constructional and electromagnetic responses of different materials which constitute the sandwich radome panels and the framework.

## **CHAPTER 2**

### **RADOMES**

#### **2.1 General Information**

The radome is a structural, weatherproof enclosure that protects a microwave or radar antenna for radar, telemetry, tracking, communications, surveillance, and radio astronomic applications [1,2]. The name “radome” is a contraction of the words “radar” and “dome” [1]. Generally, the radomes are used for protecting the antenna surfaces from harsh environmental conditions such as wind, rain, snow, ice, blowing sand, fungus, corrosion and ultraviolet rays etc. Also, they can be used for protecting nearby personnel from being accidentally struck by quickly-rotating antennas [2]. Moreover they can be used for protecting and/or concealing antenna electronic equipment from public view especially for secret security applications [2,3].

In this chapter necessity of radome is emphasized. Requirements of radomes are investigated. Different radome structures are revealed and their special properties are given. Sandwich Type Radomes are defined and their detailed properties are expressed including advantages and disadvantages. Importance of the framework geometry for the Sandwich Radomes is

discussed. Finally, structural and electromagnetic comparisons of two common framework geometries of Sandwich Radomes are expressed.

## **2.2 Necessity of Radomes**

Radome should be constructed of the material such that it protects the antenna from harsh weather conditions while minimally attenuating the electromagnetic signal transmitted or received by the antenna. In other words, the radome should be physically strong for protection and transparent to electromagnetic waves to maintain the antenna stable operation.

It is important to maintain antenna stable operation while protecting the antenna from harsh weather conditions. A radome is often used to prevent ice and freezing rain from accumulating directly onto the metal surface of the antennas. Especially for stationary antennas, excessive amounts of ice can de-tune the antenna to the point where its impedance at the input frequency rises drastically, causing voltage standing wave ratio (VSWR) to rise as well [1]. This reflected power goes back to the transmitter, where it can cause overheating. A foldback circuit activates to prevent this. However, it causes the station's output power to drop dramatically, that leads reducing its range [1].

Wind is an important factor for both stationary and spinning radar antennas. High intense wind may distort the shape and the pointing of direction of the antenna or it may cause spinning irregularities for a spinning antenna. Therefore, using radome increases pointing and tracking accuracy [3].

Rain is an important factor for high frequency radar applications. Especially above 5 GHz frequency transmission loss effect increases very rapidly. The effect leads to 10 dB transmission loss above 30 GHz. So it is important to prevent this effect for high performance antenna applications by using a radome which has hydrophobic coating feature. Detailed information about hydrophobic coating feature of radomes is given at the section 2.3.2 named as “Electromagnetic Requirements of Radomes”.

Economically, radomes are proven to be very effective when considering life cycle costs of the antenna systems. Since the antenna system is in a protected environment, maintenance costs are held to a minimum. The structural requirements of the antenna are less stringent, resulting in reduced fabrication and installation costs plus the use of smaller positioning motors [2].

As a facility, radomes provide a benign environment for any electronics and personnel that must be located near the antenna for designing or repairing applications. This is especially significant in harsh weather conditions such as temperature extremes, blowing sand or dirt, salt spray, and freezing rain [2].

Therefore it is very crucial to have radomes for high performance large radar antenna systems.

## **2.3 Requirements of Radomes**

Radomes are important parts of high frequency antenna systems. Radomes should protect antenna systems from harsh weather conditions. The design of the radome should be such that while protecting the system it should

minimally attenuate the electromagnetic signal received or transmitted by the antenna inside. We can investigate requirements of radomes in two different parts such as “mechanical requirements of radomes” and “electromagnetic requirements of radomes”.

### **2.3.1 Mechanical Requirements of Radomes**

While designing radomes it is important to decide its physical, in other words, mechanical properties. Radomes are used in different applications, such as naval applications, aircraft applications and ground applications. The place where the antenna system is constructed has to be considered and to be concentrated with its own properties at first. This consideration should include snow and rain loading, wind / gust rating, temperature of the place where the system operates, installation, transportation and repairing costs of the system.

Depending on the strength of the weather conditions on the antenna system the structure manufacturing changes. For example, generally radomes are designed to operate with wind speeds up to 60 m/s (134 mph), and snow or ice loading up to 235-kg/m<sup>2</sup> (50-lb/ft<sup>2</sup>) [4]. For an application which has higher wind speed or snow loading requirements the weight ratio of the structure has to be increased. However, enhancing structural properties of the radome may degrade electromagnetic performance of the radome if it is not properly designed.

Moreover, the nearby temperature is also an important consideration. For example, if the chosen radome is going to be used with a large radar antenna system, there should be nearby personnel to install and repair the systems. Even for the electronic equipments of the antenna there are temperature



requirements. If the antenna system is built in a cold climate, thermal insulation properties of the radome structure has higher importance.

The antenna system size may change between 1.8 m and 60 meters in diameter. To cover large antenna systems, radomes are composed of many panels. These panels are manufactured and then transported to the place of the antenna system and installed there (Figure 1 and 2). For transportation point of view the panel size is an important issue. In a typical design, panel dimensions are held to be less than 225 cm. This permits use of a standard ISO shipping container [4]. If the size increases transportation cost increases. However, these panels have to be installed at the antenna station so if the size of the radome panels decreases this time installation cost increases. So there should be an optimum decision for the radome panel size when considering cost of the radome structure.



Figure 1- Preparation of a radome panel for transportation [5]



Figure 2-Beginning, intermediate and final installation of a radome structure [6]

### **2.3.2 Electromagnetic Requirements of Radomes**

The ideal radome should appear totally transparent to any electromagnetic signal received or transmitted. Since this is not possible, radome must be designed to minimize the electromagnetic impact of itself on the enclosed antenna. This impact may be very high for antennas which have required low level side lobes. Electromagnetic requirements determine the

importance of signal distortions such as insertion loss and scattering loss of due the radome structure on the antenna system [4].

### **2.3.2.1 Insertion Loss**

In telecommunications, insertion loss is defined as the loss of signal power resulting from the insertion of a device in a transmission line or optical fiber [7]. In radome design, this means signal loss of the antenna signal due to the radome cover. Usually, it is expressed as a ratio in dB relative to the transmitted signal power, it can also be expressed as attenuation. If the power transmitted by the source is  $P_T$  and the power received by the load is  $P_R$ , then the insertion loss in dB is given by

$$IL = 10 \log_{10} \frac{P_R}{P_T} \quad (2.1)$$

### **2.3.2.2 Scattering Loss**

Scattering loss is related with IFR (Induced Field Ratio) of the antenna system. IFR is defined as the ratio of the forward scattered field to the hypothetical field radiated in the forward direction by the plane wave in the reference aperture of width equal to the shadow of the geometrical cross section of the beam/seam of the wavefront [8] (Figure 3).

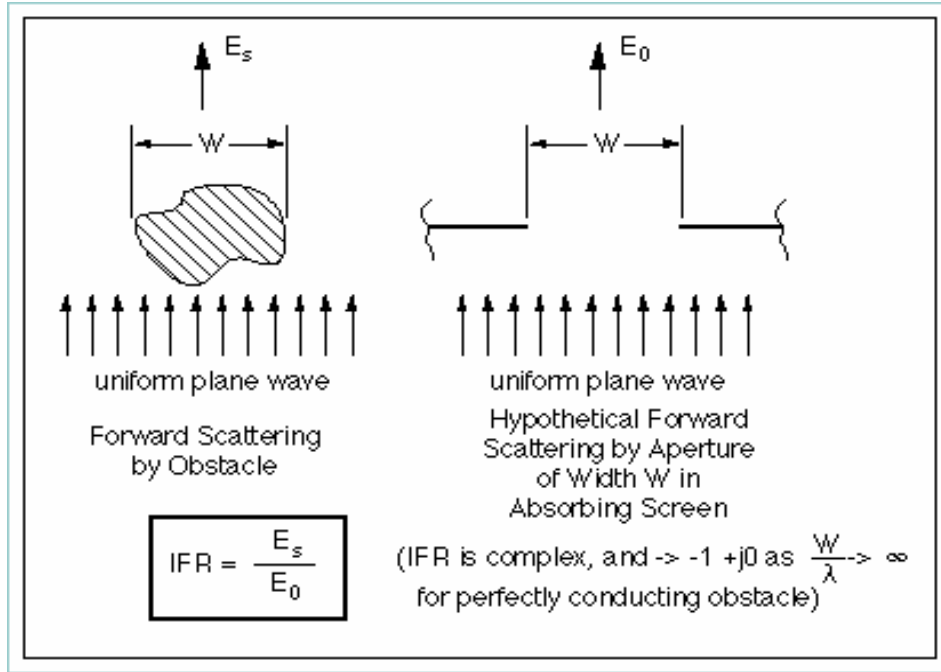


Figure 3 - Induced Field Ratio [9]

IFR is formulated as can be measured in anechoic chamber as [8];

$$IFR = (10^{0.05\Delta\alpha} e^{j\Delta\phi} - 1) \frac{e^{-j45}}{W} \sqrt{\frac{\lambda \eta_o \eta'_o}{\eta_o + \eta'_o}} \quad (2.2)$$

where  $\Delta\alpha$  in dB is the amplitude change due to obstacle in forward direction of the incident field,  $\Delta\phi$  is phase change due to obstacle in the forward direction of the incident field,  $W$  is the width of the shadow area of the obstacle's geometrical cross section on the incident wavefront,  $\lambda$  is the wavelength of the incident field,  $\eta'_o$  is the distance between the obstacle and transmitting antenna and finally  $\eta_o$  is the distance between the obstacle and the receiving antenna.

In typical radome applications insertion loss is around 0.1 dB. This loss can be adoptable. However scattering loss is much more important than the insertion loss factor. Because in antenna systems while typical radome insertion loss is around 0.1 dB, radome scattering loss may be around 10 dB for high frequency applications. Low IFR value is an indication of low scattering effect in forward direction.

Scattering loss occurs due flange framework of the radome panels. Framework scattering loss is approximately:

$$TL \approx 20 \log \left( \left| 1 + \frac{wl}{A} IFR \right| \right) \approx -8.7 \frac{wl}{A} |IFR| \quad [8] \quad (2.3)$$

where  $TL$  is the radome transmission loss (scattering loss in dB units),  $l$  is the total length of the framework,  $w$  is the framework width,  $A$  is the antenna aperture area. The  $w*IFR$  product is known as the framework electronic signature.  $w*IFR$  measurements yield two complex numbers (amplitude and phase); one where the electric field polarization is oriented parallel to the framework; and the second when the electric field polarization is perpendicular. Electronic signature  $w*IFR$  product amplitude is a measure of the effective electronic shadow width. Its value depends on the physical dimensions of the flange framework, the dielectric or inductive framework properties (dielectric or metal framework material), the details and peculiarities of the framework design shape, the antenna or radar frequency, the orientation of the framework member relative to the antenna aperture and the antenna polarization.

Note that the ratio  $w*l/A$  is the percentage framework shadow area blocking the antenna aperture area. The framework width  $w$  has structural properties consistent with the maximum rated radome wind speed specification. To enhance RF performance, a balancing act takes place between a stronger

structure with heavy-duty sized members (making  $w$  larger) and RF performance. This RF optimization process often determines that radomes are designed with minimal structural safety factors. In other words larger  $w$  values increase structural strength but decrease RF performance due to the blockage.

### **2.3.2.3 Importance of Frequency of Operation of the Antenna System**

The frequency band of the antenna system is also an important factor to be considered in a high performance radome design. The material selection for the radome is done by considering this frequency band. For example, a core material in the radome panel may have a fine insertion loss in L-Band while having inappropriate insertion loss factor at S or C Band etc. This is similarly the same case for scattering loss. For example, Metal Space Frame Radomes which have aluminum framework structure are not as impacted as the Dielectric Space Frame Radomes from the high frequency applications. Therefore, the material for radome panels and radome panel framework has to be chosen by considering the frequency band of the antenna for a high performance antenna radome design.

### **2.3.2.4 Importance of Using Hydrophobic Materials**

There is another important issue while choosing the right material for radome panels and panel flange framework. This issue is using hydrophobic materials for reducing insertion and scattering losses.

Water has a high dielectric constant and a very high loss tangent for microwave and millimeter wave frequencies. As a result, even thin films of water on the surface of antennas, radomes or feed waveguides can cause large attenuation on the transmitted or received signals.

Although use of a radome eliminates losses due to water deposited on antenna surfaces, the radome itself can allow water to collect and increase systems losses if the radome surface itself is not hydrophobic.

Hydrophobicity is measured with contact angle specification [10]. Contact angle is the angle between the surface and line drawn from the point of contact (between the surface and the water droplet) that is tangent to the water droplet as given in Figure 4. The bigger the contact angle, the more of a sphere the droplet is and the better the hydrophobic properties of the material. For example a droplet of water on a non hydrophobic surface may have a contact angle of  $15^\circ$  or even less. In general, materials which have contact angles larger than 90 degrees are expressed as hydrophobic.

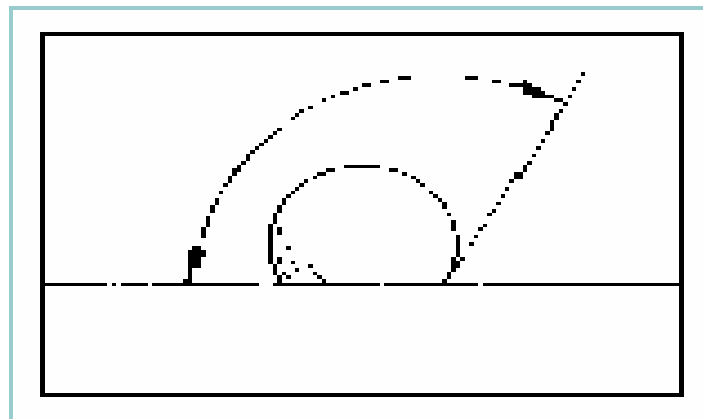


Figure 4- Evaluating Hydrophobicity by Measuring the Contact Angle of the Water Droplet on the Surface [10]

Water on the hydrophobic radome surface is in beads rather than in sheets. If the water is in beads, the energy will be slightly diffracted because the water droplets have dimensions much less than a wavelength at microwave frequencies. The responses of two different materials to the water expressed as in Figure 5. As can be seen from the figure on the hydrophobic material water is in bead form. However, on the non-hydrophobic material water is in sheet form which is typical feature of non-hydrophobicity.



Figure 5- Hydrophobic and Non-Hydrophobic Material Responses to Water

Typical hydrophobic materials are silicon dioxides, teflon based kevlar, silicon oils and fluoropolymers. Usually silicon dioxides are used in microwave antenna radome panels and flange framework to enhance hydrophobicity.



As the frequency of operation increases, impact of the water on the transmission loss (scattering loss in dB units) increases. The following figure (Figure 6) shows the importance of hydrophobic coating on the transmission losses.

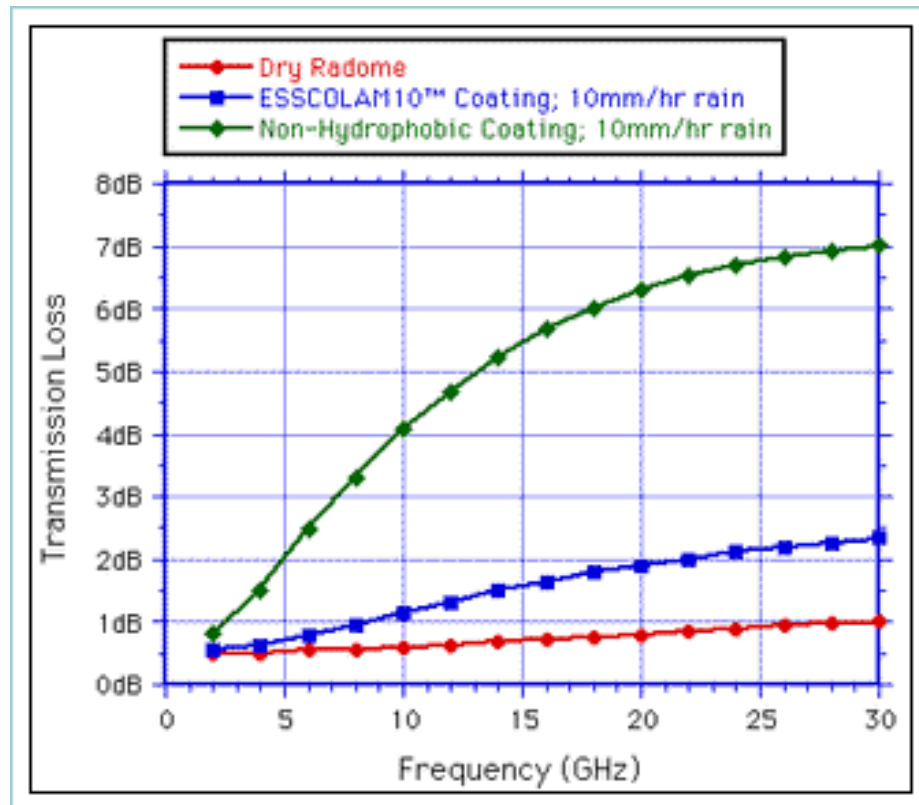


Figure 6- Effect of Hydrophobic Coating on Transmission Loss [10]

As presented in Figure 6, when the operational frequency increases up to 30 GHz frequency the transmission loss due to the 10mm/hour rain increases to 7dB for an non-hydrophobic material, however a hydrophobic material let only 2dB transmission loss due to the same rain impact. This figure clearly shows the importance of hydrophobic materials for radome applications.

## 2.4 Radome Types

There are different types of radome structures for antenna systems. Each has specific purposes, advantages considering costs, frequency of operation and dimensions of the antenna system etc.

### 2.4.1 Solid Laminate Radomes

Solid laminate radomes are used in meteorological radars, commercial satellite communications, EMI applications and fire control systems. Solid laminate radomes are suitable for applications below 3 GHz frequencies.



Figure 7 - Solid Laminate Radome for Shipboard Data Communications [3]

They are composed of doubly curved fiberglass panels, sizes of which depend on antenna size and weather conditions to stand for. The panel thickness can be changed for different applications. For high frequency applications SLR should be tuned. The tuning of a radome is defined and analyzed in Chapter 4.



Figure 8 - 3.05 m Diameter Solid Laminate Radome for MK-86 Gun Fire Control System [3]

Solid laminate radomes are usually used for smaller antenna systems when compared with DSF and MSF radomes. Usual size of SLR is between 1 and

5 meters in diameter [3]. Advantage of SLR is its cost effectiveness. However, random distribution of the panels, importance of which is presented in Chapter 4 is impossible for solid laminate radomes. This leads to greater boresight and side lobe degradation and this is the main limit of usage for high performance applications with solid laminate radomes [3].

### **2.4.2 Dielectric Space Frame Radomes**

Dielectric space frame radomes are usually used for low frequency communications and EMI test applications under 1 GHz. The framework structure of DSF is usually made of fiberglass [3]. Usage of fiberglass for a framework structure in DSF radomes prevents corrosion problems in harsh and salt environments.



Figure 9 - Dielectric Space Frame Radome [2]

The panels are composed of membranes which are pre-stressed to form a rigid panel. The pre-stress process eliminates wavy, flapping panel membranes and eliminates the need for pressurization to reduce oil-canning, sound/vibration noise, microphonics and fatigue failure characteristics etc. [2]. The panels can be in regular geometries or randomized geometries. Size of DSF radomes depends between 1.8 meters and 20 meters in diameter [3]. For large antenna systems to cover the antenna larger beams of fiberglass framework is required for structural reasons and this leads performance degradation. Therefore for high frequency applications in general DSF is a not logical choice. However, the electromagnetic performance of DSF can be enhanced by tuning the dielectric framework structure as defined and analyzed in Chapter 4. This technique broadens the frequency band of operation of the DSF radomes.

### **2.4.3 Metal Space Frame Radomes**

Metal space frame radomes are usually used in military and commercial satellite communications, intelligence gathering, radio astronomy, weather radars and 2-D surveillance radars [3]. Usual panel shapes are triangular in MSF radomes as presented in Figure 10. These panels are bolted together to form a geodesic dome. The framework structure of MSF is made of aluminum. Aluminum has more powerful mechanical properties than fiberglass used in DSF structures. This property lets using thin beams of aluminum for framework of the panels which minimizes scattering loss of the radome.



Figure 10- 14.1 m Diameter Metal Space Frame Radome [3]

It is one of most common radomes in antenna engineering. Because MSF radomes are used between 0.5 GHz and 100 GHz with high performances and this feature makes them unique. Even there are examples of usage up to 1000 GHz with high performance panels [3]. This is an important advantage when compared with Dielectric Space Frame radomes. Another advantage of Metal Space Frame radome is the size of the radome structure. Since the elastic modulus of the framework material is quite high, it is possible to design MSF radomes up to 60 meters in diameter using thin beams of Aluminum for the framework structure. Moreover thickness of triangular panels can be varied by considering the structural performance and the

operating frequency of the antenna system to have optimum characteristics by minimizing insertion loss of the radome structure.

#### **2.4.3.1 Structural Comparison of Dielectric Space Frame Radomes and Metal Space Frame Radomes**

Both Dielectric Space Frame (DSF) and Metal Space Frame (MSF) radomes are assembled from many panels, which are composed of a structural framework with attached thin membrane walls. For the Dielectric Space Frame (DSF) radome, the radome panel framework and rigid membrane walls are laminated one piece monolithic units manufactured from Fiberglass Reinforced Plastic (FRP) materials. The panel flanges form the radome framework. In contrast for the Metal Space Frame (MSF) radome, the thin membrane wall is attached to an Aluminum metal framework. To accomplish the attachment process, the membrane material must be very pliable. The usual panel material choice is Dacron in MSF radomes [2]. While dielectric space frame FRP radomes have a rigid membrane wall, a Dacron membrane wall in metal space frame radome is easily recognizable by flapping panel membranes. At moderate wind speed levels, Metal Space Frame radomes have to require pressurization to reduce membrane oil-canning, sound/vibration noise, microphonics and fatigue failure. The panel membrane material has a significant and major role in determining the strength of the radome structure. Although the framework material of the Metal Space Frame radome Aluminum is much stronger than Fiberglass Reinforced Plastic (FRP) material, which is the core material of Dielectric Space Frame radome, MSF is weaker than DSF. This is the reason of structural degradation effect of panel membranes of MSF. Dielectric Space Frame radomes are stronger than the Metal Space Frame radomes to the

harsh weather conditions such as wind and corrosion with the well-built panel membranes.

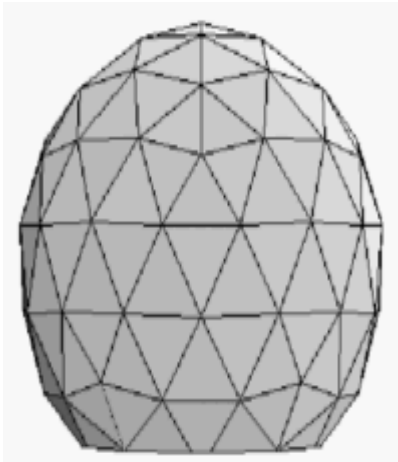
Considering structural strength of the radome types usually there are two parameters in the literature. They are critical buckling wind speed and safety factor. Critical buckling wind speed shows the maximum wind speed that the radome can be sustained safely. Safety factor shows the radome structural performance in a fixed wind speed. For a structural point of view, high values for critical buckling wind speed and safety factor shows the strength of the radome structure. It is a figure of merit for considering structural performances of radomes.

Table 1 demonstrates the critical buckling speed and safety factor for identical 41ft (12.6m) space frame radomes. In each case, the framework member size (width and depth) is the same for both radome types. Only Aluminum material properties are substituted for the FRP material in DSF and Dacron thin membrane wall material properties are substituted for FRP in DSF. As presented at the table the dielectric space frame radome is 150 percent stronger than the metal space frame unit. While the dielectric space frame radome 2.5 safety factor is adequate for a 323 km/hr wind speed requirement, the equivalent metal space frame radome has only a 1.0 safety factor. The only way for the metal space frame radome to safely meet a 323 km/hr specification wind speed is to increase the Aluminum framework member size or change the membrane to a stronger material. Since a flexible membrane material is necessary for the fabrication of the metal space frame panel, there is little choice but to stay with Dacron. Therefore, only decision available for the metal space frame radome is increasing the Aluminum framework member size. There is, however, a penalty to pay for increasing the Aluminum framework size. This penalty comes in the form of a



simultaneous increase in transmission loss and deterioration of RF performance.

Table 1- Structural Comparison of Metal Space Frame Radomes and Dielectric Space Frame Radomes [2]

<b>Radome Design Parameter</b>	<b>Dielectric Space Frame Radome (DSF)</b>	<b>Metal Space Frame Radome (MSF)</b>	<b>Typical Space Frame Radome Picture</b>
<b>Flange Framework Material</b>	<b>FRP</b>	<b>Aluminum</b>	
<b>Panel Membrain Material</b>	<b>FRP</b>	<b>Dacron</b>	
<b>Critical Buckling Wind Speed</b>	<b>509 km/h</b>	<b>323 km/h</b>	
<b>Safety Factor at 320 km/h Wind Speed</b>	<b>2.50</b>	<b>1.01</b>	

#### **2.4.4 Air Pressurised Radomes**

Air pressurised radomes are the easiest type of radomes considering implantation of a radome structure. They resemble like pressurised balloons. Figure 11 represents a typical installation of an air pressurized radome structure. Inside air pressurised radomes there are inflation blowers for pressurising operation. The mechanical protection of the antenna system is gathered by pressurising the cover coating at a variant pressure optimized for outside wind speed. There is no flange framework for this radome as presented in figure 11. Outermost radome structure is composed of just the teflon based cover protecting the antenna system inside.

The frequency performance of operation totally depends on the electromagnetic characteristics of the material used in radome cover. Usual applications of these type radomes are below 20 GHz. They are easily implantable and transportable. However, the mechanical properties are less powerful than other type of radome structures. They are suitable for low cost and low period usage system designs.



Figure 11- Beginning, Intermediate and Final Installations of Air Pressurised Radome [11]

## 2.5 Sandwich Type Radomes

Sandwich type radomes are used for high performance, discrete narrow bandwidth large antenna system applications as seen in Figure 12. Typical applications where the sandwich type radomes have been used are 3-D military and commercial radar applications, air traffic controlling and other radar systems such as weather radar, phased array radar, secondary surveillance radar etc [3]. Sandwich type radomes are very important especially for discrete narrow band applications.



Figure 12 -Sandwich Type Radome with Large Access Doors [3]

### 2.5.1 Features of Sandwich Type Radomes

Sandwich type radomes have multi layered geometrical construction. This property totally differs them from other types of radomes. Three layer sandwich radomes are named as Type-A Sandwich Radomes and they are the most common sandwich type. There are also three layered sandwich radomes which have core materials at inner and outermost part of the radome named as Type-B and there are five layered sandwich radomes which are named as Type-C Sandwich Radomes as seen in Figure 13.

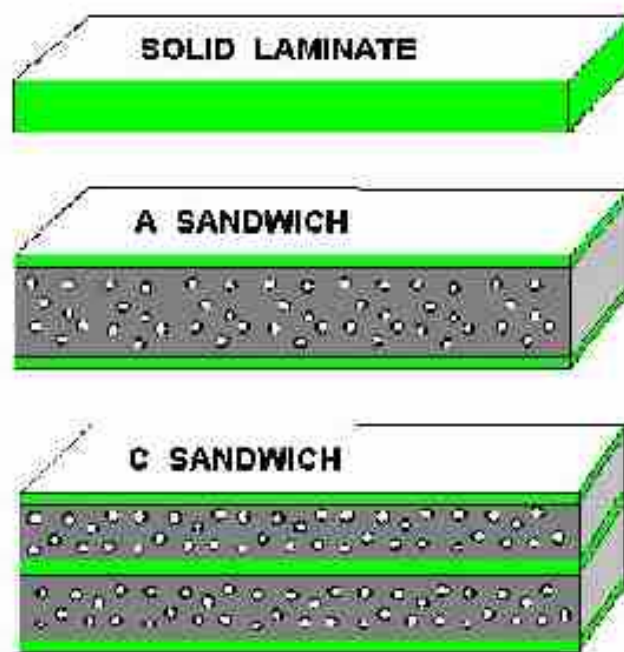


Figure 13- Sandwich Radome Types [13]

The name “sandwich” comes from the multi-layered structure of the radome. Sizes of sandwich radomes may change between 3 and 24 meters in diameter [3]. Multi-layered polygonal panels on sandwich radomes are bolted together to form truncated sphere radome geometry. Panels have highly composite materials which increase consistency and mechanical strength of the radome structure. Outermost and inner most surfaces of the panels are made of fiberglass. Main core of the panel structure include composite honeycomb materials such as Kevlar, Polyurethane, Resin filled 3D-glass, etc. Some examples of the materials are given in Figure 14 and Figure 15. Main core is the main part of creation of temperature difference between inside an outside. Thickness of the main core depends on the requirement level of the protection of antenna system and antenna personnel inside for harsh weather conditions.



Figure 14- 3D Glass Material Used in Core Part of Type-A Sandwich Radomes [19]

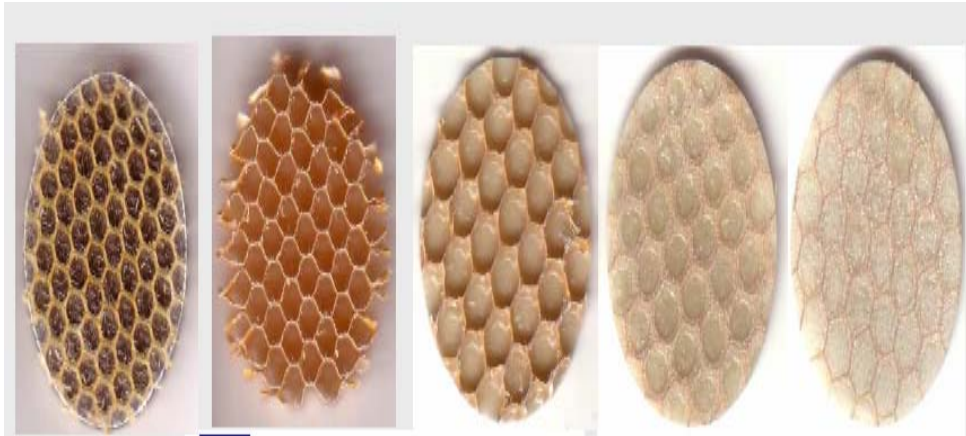


Figure 15- Honeycomb Core Materials Used in Type-A Sandwich Radomes [19]

Smith chart is also useful when determining optimum thickness of sandwich radomes. Besides thermal insulation property, foam core increases water rejection properties and also provides greater impact strength and consistent, high radar transparency without sacrificing weight and structural stability, thereby providing a much longer service life in moisture/impact critical environments. Also, thickness of the foam core can be arranged to have optimum insertion loss characteristics considering the specific frequency band of operation of the antenna system inside which increases radar transparency of sandwich type radomes.

Multi layered panels on the sandwich radomes are attached each other by seams as in figure 16. As expressed before because of shipping and transportation issues large antenna radomes have to be composed of different panels. The framework is composed of the seams which are the structures which put these highly composite multi layered panels together in sandwich type radomes. Electromagnetic importance of seams in sandwich type radomes are investigated in section 2.5.4.



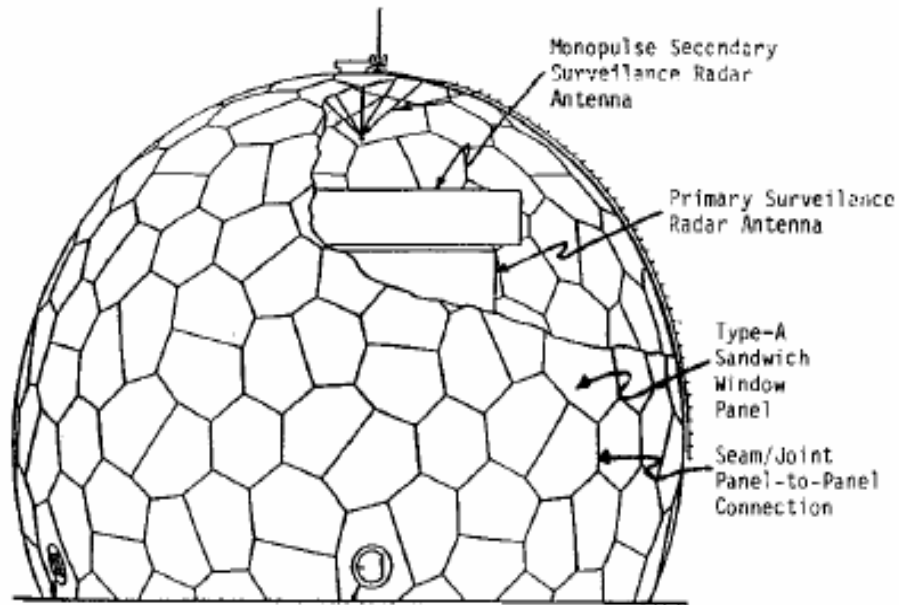


Figure 16- Sandwich Radome Panels and Framework Geometry

### 2.5.2 Advantages of Sandwich Type Radomes

Sandwich radomes have excellent electromagnetic performance at specific discrete narrow band applications. As presented in Chapter 4 tuning operation on the framework structure enhances electromagnetic transparency of the radome system. This increases usage of sandwich type radomes even for high frequency applications just like metal space frame radomes.

Skin and core thickness can be varied for optimum performance at operating frequency for sandwich type radomes. Moreover, if there are critical low level side lobes for antenna, sandwich radome is excellent choice by the



arrangement property of panel thickness and seam geometry. Also, panel removal and repair is much easier than other radome types.

### **2.5.3 Disadvantages of Sandwich Type Radomes**

There are some drawbacks of sandwich type radomes. Geometric design before implantation is very critical for sandwich radomes because tooling is required for each changing size. Moreover, electromagnetic performance is frequency discrete [3]; in other words they don't give high performance for large frequency bands of operation. For example, a sandwich radome design for an antenna operating at 5 GHz may not be used as the same performance with the same antenna dimensions for 20 GHz. Furthermore, manufacturing tolerance of panels and joint design of the panels by the seams is very critical to have high performance designs. These features make sandwich type radomes the most expensive solution among other type of radome types.

### **2.5.4 Importance of Framework Structures in Sandwich Type Radomes**

Sandwich radome multi layered panels are attached each other by the seams. These seams constitute the framework structure of the sandwich type radomes. The physical dimensions of the seams are usually determined by structural considerations, such as maximum wind speed and the resultant stress that the seams have to sustain. However, without electromagnetic

consideration the seams may degrade total system performance by introducing high scattering values [12].

Panels of sandwich radomes are specially manufactured to have minimum insertion loss at required insulation values. Typical transmission loss of the panels is around 0.1 dB depending on the discrete frequency of operation. However, the scattering loss of the framework of the panels (seams) maybe 4 to 100 times greater without electromagnetic consideration. To have high performance sandwich radome design, electromagnetic analysis of the seam structure has to be done at first. Then to minimize the scattering effect of seam structure, solutions have to be found. The following chapter (chapter 3) is devoted to the electromagnetic analysis of the framework of the sandwich type radomes. In chapter 4, to enhance electromagnetic transparency of sandwich type radomes different design methods are presented and investigated.

### **2.5.5 Structural and Electromagnetic Comparison of Different Sandwich Radome Framework Geometries**

As expressed in this chapter the radome must be packaged for shipment for worldwide transportation. What this means is that the maximum panel size must conform to standard shipping sizes. Therefore it should be designed such that the whole radome has to be composed of panels which are transported to the place of the antenna system and installed there. Taking into account shipping size constraints, two common sandwich radome framework geometry types can be found in the market, which are the symmetric orange peel and quasi-random geometries shown in Figures 17 and Figure 18, respectively.

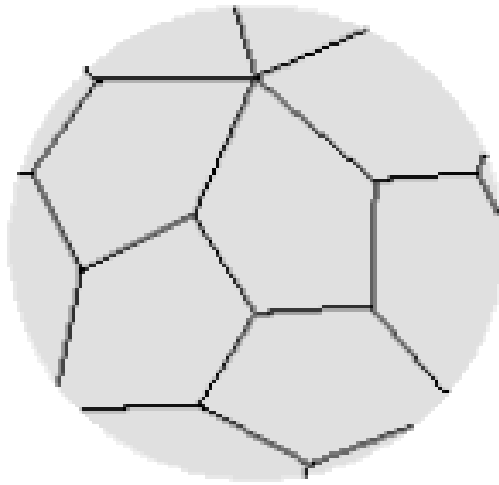


Figure 17- Typical Quasi Random Sandwich Radome Geometry

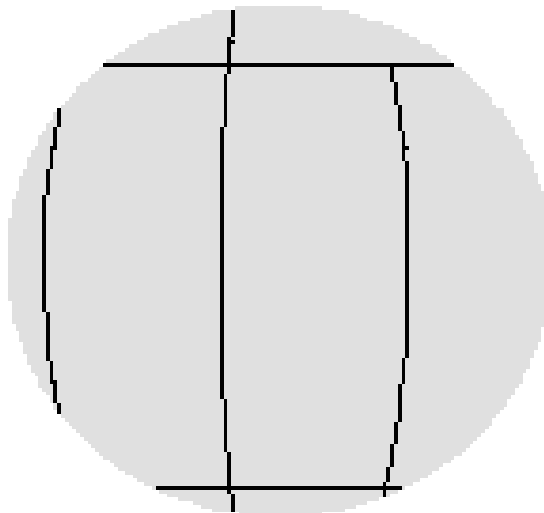


Figure 18 – Typical Orange Peel Sandwich Radome Geometry

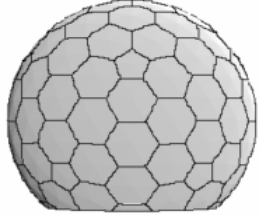

Quasi-random geometrical sandwich radomes may have triangular, hexagonal or pentagonal panel shapes. A geodesic radome using triangular panels is an alternate implementation of the quasi-random radome geometry. Orange peel radome panels have usually flat planes for production and installation easiness. Usually they have lower cost and they are used for low budget antenna systems.

Quasi-random geometrical sandwich radome structures have important electromagnetic transparency properties while compared with orange-peel type sandwich radomes. As discussed in Chapter 4 the scattering electromagnetic field components of each sandwich radome seam should not be added directly to have high total scattered field components which have important effects especially on low side lobe levels of the original antenna electromagnetic field. In quasi-random type sandwich radome structures, since the seam geometries are distributed in arbitrary direction the cumulative effect is very low while compared with the orange-peel type geometries.

There are also structural issues for design considerations between two different sandwich radome types, because the main aim of the radome is to protect the antenna from harsh weather conditions. Table 2 is a structural comparison between Quasi-Random geometrical sandwich radome and Orange-Peel geometrical sandwich radome type for 10.7m diameter length. This table shows that quasi-random radome geometry is significantly stronger than the symmetric orange peel geometry. The quasi-random radome is 119 percent stronger than the symmetric orange peel unit and has an appropriate safety factor of 2.19 for a 240km/hr specification wind speed. In contrast, the symmetric orange peel radome only has 240km/h critical buckling speed and a safety factor of 1.0. Therefore using Quasi-Random

geometric structures in sandwich radomes enhances both electromagnetic and structural performances of the system.

Table 2- Structural Comparison of Quasi Random Sandwich Radome Geometry and Orange-Peel Sandwich Radome Geometry

<b>Radome Geometry</b>	<b>Critical Buckling Wind Speed</b>	<b>Safety Factor At 240 km/h Wind Speed</b>	<b>Typical Radome Geometry Scheme</b>
<b>Quasi-Random</b>	<b>357 km/hr</b>	<b>2.19</b>	
<b>Orange Peel</b>	<b>241km/h</b>	<b>1.00</b>	

## **CHAPTER 3**

# **ELECTROMAGNETIC SCATTERING ANALYSIS OF SEAMS IN SANDWICH TYPE RADOMES**

### **3.1 General Information**

In this chapter electromagnetic scattering analysis of sandwich radome is presented. In the analysis, electromagnetic scattering from the arbitrary distributed radome seams are analyzed. For the purpose of computing the scattering electromagnetic field from the seams of sandwich radomes, it is required to imitate the seams to a known geometrical object with certain properties. For example in [12] scattered electromagnetic field is obtained by assuming the sandwich radome seams as perfectly conducting strips that radiate with the given incident field of the antenna. In this thesis work, sandwich radome seams are assumed to be circular cylinders which are composed of conducting cylinders coated with dielectrics to have close assumption for the real case of tuned sandwich radome seam structure which is presented in Chapter 4. In the analysis, lengths of the cylinders are assumed as infinite, since they are placed in the near zone and block the aperture of the antenna. To formulate the scattering field from the seams, there is also need to know the near field of the antenna covered by the

sandwich radome [12]. Analysis technique in this thesis work is applicable for all types of antenna systems with the condition of knowledge of near and far electromagnetic field formulations of the systems. Analysis in this thesis work is done for a transmitting antenna covered by the sandwich radome such that near incident field of the antenna is scattered from the framework structure and constitute total far electromagnetic fields with antenna original far field together. For the reciprocal case of a receiving antenna, this analysis is valid with the condition of knowledge of incident fields on the framework structure of the sandwich radome.

In the analysis, pyramidal horn type antenna is used as a transmitting antenna as a case study. The effect of scattering is emphasized by comparing total far electromagnetic field of the antenna and radome structure together with far electromagnetic field of the antenna without radome structure. Finally, total far electromagnetic field is expressed as the summation of antenna far electromagnetic field and the scattered field due to radome structure for both transverse electric and transverse magnetic incident field radiation by the antenna inside the sandwich radome.

### **3.2 Scattering Analysis of Radome Seams**

In the scattering analysis, after having the assumptions for the physical and geometrical assumptions of the seam structure, there exists another requirement which is information on near electromagnetic field of the antenna system inside the radome. Near electromagnetic field of the antenna system is required to define the incident field to obtain the scattered electromagnetic field from the seam structure. This combination gives the enough information to define the scattered field from the seam structure of a sandwich radome [12],[17]. In this section the analysis is done considering

single seam, in the next section, this analysis is generalized for arbitrary distributed M number of sandwich radome seams.

The scattered E-Field from the sandwich radome seam [18] can be explained as:

$$E_s = E_{incident} f(r, \phi', \psi) \quad (3.1)$$

where  $E_s$  represents electric field scattered by the seam in the far zone,  $E_{incident}$  represents the incident field generated by the antenna.  $f(r, \phi', \psi)$  is the function that relates the incident electric field to the scattered electric field by the seam structure. In this function  $r$  represents the distance from the point  $P$ , where the far-electromagnetic field is gathered to the axis of sandwich radome seam which is considered in cylindrical geometry as presented in Figure 19.  $\phi'$  represents the angle of this far field point with the x-axis.  $\psi$  represents the angle between incident propagating electromagnetic field generated by the antenna and cylinder axis normal. For example, if  $\psi = 0$ , this shows a normal incidence of electromagnetic field to the sandwich radome seam, if  $\psi \neq 0$ , this shows an oblique incidence to the sandwich radome seam as presented in Figure 19.



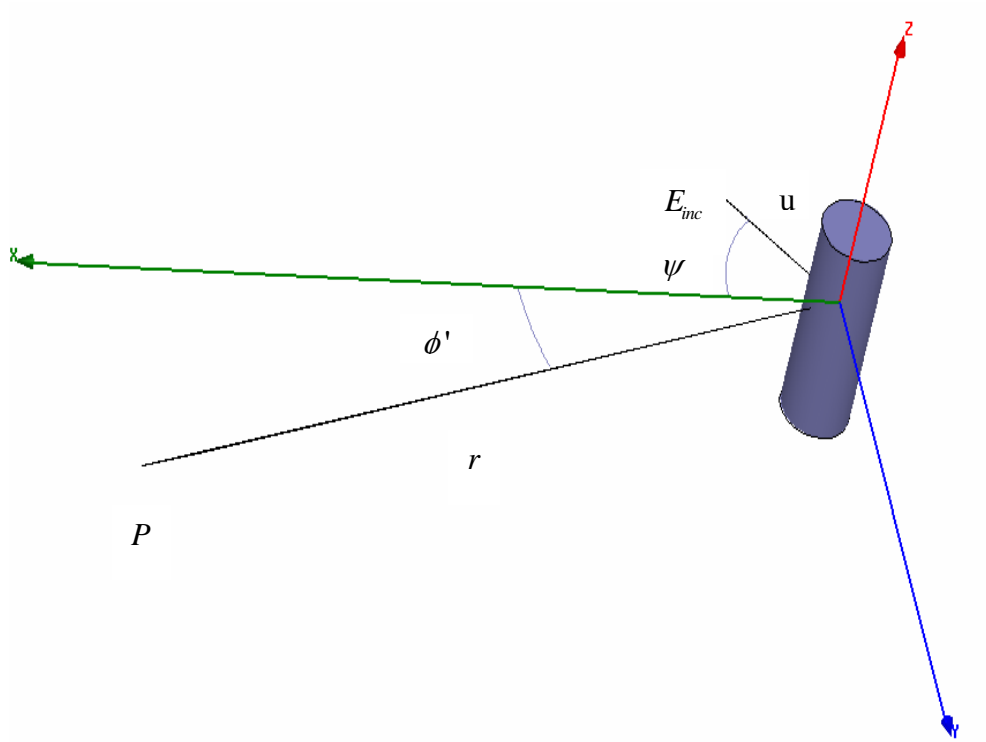


Figure 19 - Scattering Geometry of the Analysis

It is assumed that dielectric coated perfectly conducting cylinder with a total radius of  $a_0$  is positioned along z-axis. Considering the same geometry transverse electric (TE) and transverse magnetic (TM) analysis is done separately.

In the TE analysis, it is assumed that TE incident field of radiation is generated by the antenna. Scattered electromagnetic field by the coated cylinder  $E^{sTE}$  is expressed as [18] :

$$E^{sTE} = E_{inc}^{TE} f(r, \phi', \psi) \quad (3.2)$$

Scattered electric field from the seam structure can be decomposed into the vector coefficients such as  $E_z^{sTE}$  and  $E_\phi^{sTE}$  as [18] :

$$E_z^{sTE} = E_{inc}^{TE}(\cos\psi)(e^{jk_0 z \sin\psi}) \sum_{n=-\infty}^{n=\infty} (-j)^n C_n H_n^{(1)}(k_0 r \cos\psi) e^{jn\phi'} \quad (3.3)$$

$$\begin{aligned} E_\phi^{sTE} = & E_{inc}^{TE}(\cos\psi)(e^{jk_0 z \sin\psi}) \\ & \sum_{n=-\infty}^{n=\infty} (-j)^n [C_n H_n^{(1)}(k_0 r \cos\psi) \frac{(-n \sin\psi)}{k_0 r \cos^2\psi} \\ & + \frac{j}{\cos\psi} C_n^{TE} H_n^{(1)'}(k_0 r \cos\psi)] e^{jn\phi'} \end{aligned} \quad (3.4)$$

where  $H^{(1)}$  is the Hankel function of the first kind, and  $k_0$  is the wave number such as  $k_0 = \omega\sqrt{\mu_0\epsilon_0}$ . Primes in Hankel functions represent the derivation of the function.  $C_n$  and  $C_n^{TE}$  are the series coefficients given below:

$$C_n^{TE} = -\frac{M_n N_n - q_n^2 J_n(x_0) H_n^{(1)}(x_0)}{P_n N_n - [q_n H_n^{(1)}(x_0)]^2} \quad (3.5)$$

$$C_n = j \frac{2}{\pi x_0} \left[ \frac{s_0 q_n}{P_n N_n - [q_n H_n^{(1)}(x_0)]^2} \right] \quad (3.6)$$

where  $x_0$ ,  $q_n$  and  $s_0$  are expressed as:

$$x_0 = k_0 a_0 \cos\psi \quad (3.7)$$

$$q_n = \frac{n \sin \psi}{k_0 a_0} \left( \frac{1}{\varepsilon_r \mu_r - \sin^2 \psi} - \frac{1}{\cos^2 \psi} \right) \quad (3.8)$$

$$s_0 = \frac{1}{\cos \psi} \quad (3.9)$$

and  $\varepsilon_r, \mu_r$  are the relative permittivity and permeability coefficients of the coated cylinder, respectively.

where  $P_n, M_n, N_n$  appearing in above equations are defined as:

$$P_n = H_n^{(1)}(x_0) - Y_n H_n^{(1)'}(x_0) \quad (3.10)$$

$$M_n = J_n(x_0) - Y_n J_n'(x_0) \quad (3.11)$$

$$N_n = H_n^{(1)}(x_0) - Z_n H_n^{(1)'}(x_0) \quad (3.12)$$

where  $Y_n$  and  $Z_n$  are expressed as:

$$Y_n = \frac{s_0}{r_1} \frac{J_n(x_1) H_n^{(1)'}(x_2) - H_n^{(1)}(x_1) J_n'(x_2)}{J_n'(x_1) H_n^{(1)'}(x_2) - H_n^{(1)'}(x_1) J_n'(x_2)} \quad (3.13)$$

$$Z_n = \frac{s_0}{s_1} \frac{J_n(x_1) H_n^{(1)}(x_2) - H_n^{(1)}(x_1) J_n(x_2)}{J_n'(x_1) H_n^{(1)}(x_2) - H_n^{(1)'}(x_1) J_n(x_2)} \quad (3.14)$$

where  $a_1$  represents radius of the perfectly conducting part and  $a_0$  is the total radius of the coated cylinder with,

$$x_1 = k_0 a_0 \sqrt{\mu_r \varepsilon_r - \sin^2 \psi} \quad (3.15)$$

$$x_2 = k_0 a_1 \sqrt{\mu_r \varepsilon_r - \sin^2 \psi} \quad (3.16)$$

$$r_1 = \frac{\mu_r}{\sqrt{\mu_r \varepsilon_r - \sin^2 \psi}} \quad (3.17)$$

$$s_1 = \frac{\varepsilon_r}{\sqrt{\varepsilon_r \mu_r - \sin^2 \psi}} \quad (3.18)$$

Near incident field of the antenna is taken from a pyramidal horn type antenna as a case study. Horn antenna is assumed to have small flare angle such that uniform phase distribution on the aperture is obtained. Moreover, it is assumed that antenna aperture field distributions are not affected with sandwich radome seams placed in the near field of the antenna.

There are different ways for calculating near field of horn type antennas. For example, aperture of the antenna can be divided into minimized sub-apertures. Summation of the far field distributions of these sub-apertures constitutes the near field of the horn antenna. Also, near field of the horn antenna can be related with the input power, gain of the antenna and the distance where the near field is obtained such that near field of the horn antenna can be taken as [16] :

$$E_{incident} = \sqrt{\frac{\eta_0 P G}{4\pi}} \frac{1}{u} \quad (3.19)$$

where  $E_{incident}$  represents near field of the antenna,  $\eta_0$  is the free space wave impedance,  $P$  is the input power of the antenna,  $G$  is the power gain of the antenna and  $u$  is the distance of the seam from the aperture as presented in figure 19.

$G$  can be taken as [16] :

$$G = 21,6 f a \quad (3.20)$$

where  $f$  is the operating frequency of the antenna in Gigahertz and  $a$  is the larger of the two cross-sectional dimensions of the aperture in meters.

Finally scattered transverse electric far electromagnetic field of the antenna and sandwich radome seam is found as follows:

$$\begin{aligned} \vec{E}^{sTE} = & \left[ \sqrt{\frac{\eta_0 P 21,6 f a}{4\pi}} \frac{1}{u} \cos \psi e^{jk_0 z \sin \psi} \right] \\ & \left[ \sum_{n=-\infty}^{n=\infty} (-j)^n C_n H_n^{(1)}(k_0 r \cos \psi) \frac{(-n \sin \psi)}{k_0 r \cos^2 \psi} + \right. \\ & \left. \frac{j}{\cos \psi} C_n^{TE} H_n^{(1)'}(k_0 r \cos \psi) \right] e^{jn\phi'} \hat{a}_\phi \\ & + \sum_{n=-\infty}^{n=\infty} (-j)^n C_n H_n^{(1)}(k_0 r \cos \psi) e^{jn\phi'} \hat{a}_z \quad (3.21) \end{aligned}$$

Transverse magnetic (TM) wave scattered from the sandwich radome seam is analyzed similarly assuming incident radiation from the inside antenna as the following [18]:

$$E_z^{sTM} = E_{inc}^{TM} (\cos \psi) (e^{jk_0 z \sin \psi}) \sum_{n=-\infty}^{n=\infty} (-j)^n C_n^{TM} H_n^{(1)}(k_0 r \cos \psi) e^{jn\phi} \quad (3.22)$$

$$\begin{aligned} E_\phi^{sTM} = & E_{inc}^{TM} \cos \psi e^{jk_0 z \sin \psi} \\ & \sum_{n=-\infty}^{n=\infty} (-j)^n [C_n^{TM} H_n^{(1)}(k_0 r \cos \psi) \frac{(-n \sin \psi)}{k_0 r \cos^2 \psi} \\ & - \frac{j}{\cos \psi} \sqrt{\frac{\mu_0}{\epsilon_0}} C_n H_n^{(1)'}(k_0 r \cos \psi)] e^{jn\phi} \end{aligned} \quad (3.23)$$

where  $C_n^{TM}$  is expressed as the following:

$$C_n^{TM} = -\frac{V_n P_n - q_n^2 J_n(x_0) H_n^{(1)}(x_0)}{P_n N_n - [q_n H_n^{(1)}(x_0)]^2} \quad (3.24)$$

with,

$$V_n = J_n(x_0) - Z_n J_n'(x_0) \quad (3.25)$$

Finally, scattered transverse magnetic field of the antenna and sandwich radome structure is found to be:

$$\begin{aligned}
\vec{E}^{sTM} = & E_{inc}^{TM} \cos \psi e^{jk_o z \sin \psi} \sum_{n=-\infty}^{n=\infty} (-j)^n C_n^{TM} H_n^{(1)}(k_0 r \cos \psi) e^{jn\phi'} \hat{a}_z + \\
& E_{inc}^{TM} \cos \psi e^{jk_o z \sin \psi} \sum_{n=-\infty}^{n=\infty} (-j)^n [C_n^{TM} H_n^{(1)}(k_0 r \cos \psi) \left( \frac{-n \sin \psi}{k_0 r \cos^2 \psi} \right) \\
& \left( \frac{-j}{\cos \psi} \right) \sqrt{\frac{\mu_0}{\epsilon_0}} C_n H_n^{(1)}(k_0 r \cos \psi)] e^{jn\phi'} \hat{a}_\phi
\end{aligned}
\tag{3.26}$$

### 3.3 Total Far Field Expression of Antenna and Arbitrary Distributed Sandwich Radome Seams

Total far electric field of the antenna and radome structure composition is the summation of antenna far electric field without radomes and total scattered far electromagnetic field due to the arbitrary distributed radome seams as expressed in the following equation.

$$\vec{E}_{Total} = \vec{E}_{Antenna} + \vec{E}_{Scattered} \tag{3.27}$$

In this equation  $\vec{E}_{Total}$  represents total far electric field of antenna and radome framework structure composition,  $\vec{E}_{Antenna}$  represents original antenna far electric field and  $\vec{E}_{Scattered}$  represents total scattered electric field from the framework structure of sandwich radomes.

In this section, total scattered field is analyzed first, then total far electric field of the antenna system which is generated by the antenna and the scattered field from the sandwich radome framework structure is found and simulated.

To obtain a general solution for seam scattering, the analysis done in previous section is generalized including the arbitrary distributed seams in front of the antenna system. Assume the angle between incident propagating electromagnetic field and the  $m^{th}$  sandwich radome seam is given as  $\psi_m$ . Assuming there are M radome seams, far electromagnetic scattered field by the arbitrary distributed sandwich radome seams is expressed as:

$$\begin{aligned}
E_{\phi}^{sTE} = & \sum_{m=1}^M E_{inc}^{TE}(\cos \psi_m)(e^{jk_0 z \sin \psi_m}) \\
& \sum_{n=-\infty}^{n=\infty} (-j)^n [C_n H_n^{(1)}(k_0 r \cos \psi_m) \frac{(-n \sin \psi_m)}{k_0 r \cos^2 \psi_m} \\
& + \frac{j}{\cos \psi_m} C_n^{TE} H_n^{(1)'}(k_0 r \cos \psi_m)] e^{jn\phi'} \quad (3.28)
\end{aligned}$$

$$\begin{aligned}
E_z^{sTE} = & \sum_{m=1}^M E_{inc}^{TE} \cos \psi_m e^{jk_0 z \sin \psi_m} \\
& \sum_{n=-\infty}^{n=\infty} (-j)^n C_n H_n^{(1)}(k_0 r \cos \psi_m) e^{jn\phi'} \quad (3.29)
\end{aligned}$$

$$C_n^{TE} = -\frac{M_n N_n - q_n^2 J_n(x_0) H_n^{(1)}(x_0)}{P_n N_n - [q_n H_n^{(1)}(x_0)]^2} \quad (3.30)$$



$$C_n = j \frac{2}{\pi x_0} \left[ \frac{s_0 q_n}{P_n N_n - [q_n H_n^{(1)}(x_0)]^2} \right] \quad (3.31)$$

where  $x_0$ ,  $q_n$  and  $s_0$  are expressed as:

$$x_0 = k_0 a_0 \cos \psi_m \quad (3.32)$$

$$q_n = \frac{n \sin \psi_m}{k_0 a_0} \left( \frac{1}{\varepsilon_r \mu_r - \sin^2 \psi_m} - \frac{1}{\cos^2 \psi_m} \right) \quad (3.33)$$

$$s_0 = \frac{1}{\cos \psi_m} \quad (3.34)$$

Also note that since far electromagnetic field scattering is analyzed here, the distance  $r$  between the seams and far electromagnetic field measurement point is taken the same with the assumption of all the seams in the near field are close each other compared with the far field distances. Same claim is valid for the angle  $\phi'$ . Since the scattered field is gathered far away from the seam structures, the angle  $\phi'$  is kept as same for distributed sandwich radome seams which are close each other when compared with the far field distances.

$\varepsilon_r$ ,  $\mu_r$  are the relative permittivity and permeability of the coated cylinder shown in Figure 19.

where  $P_n, M_n, N_n$  is defined as:

$$P_n = H_n^{(1)}(x_0) - Y_n H_n^{(1)'}(x_0) \quad (3.35)$$

$$M_n = J_n(x_0) - Y_n J_n'(x_0) \quad (3.36)$$

$$N_n = H_n^{(1)}(x_0) - Z_n H_n^{(1)'}(x_0) \quad (3.37)$$

where  $Y_n$  and  $Z_n$  are expressed as:

$$Y_n = \frac{s_0}{r_1} \frac{J_n(x_1) H_n^{(1)'}(x_2) - H_n^{(1)}(x_1) J_n'(x_2)}{J_n'(x_1) H_n^{(1)'}(x_2) - H_n^{(1)'}(x_1) J_n'(x_2)} \quad (3.38)$$

$$Z_n = \frac{s_0}{s_1} \frac{J_n(x_1) H_n^{(1)}(x_2) - H_n^{(1)}(x_1) J_n(x_2)}{J_n'(x_1) H_n^{(1)}(x_2) - H_n^{(1)'}(x_1) J_n(x_2)} \quad (3.39)$$

where  $a_1$  represents radius of the perfectly conducting part and  $a_0$  is the total radius of the  $m^{th}$  coated cylinder with,

$$x_1 = k_0 a_0 \sqrt{\mu_r \varepsilon_r - \sin^2 \psi_m} \quad (3.40)$$

$$x_2 = k_0 a_1 \sqrt{\mu_r \varepsilon_r - \sin^2 \psi_m} \quad (3.41)$$

$$r_1 = \frac{\mu_r}{\sqrt{\mu_r \varepsilon_r - \sin^2 \psi_m}} \quad (3.42)$$

$$s_1 = \frac{\varepsilon_r}{\sqrt{\varepsilon_r \mu_r - \sin^2 \psi_m}} \quad (3.43)$$

Then, total transverse electric scattered field is found as:

$$\begin{aligned} \vec{E}_{Scattered}^{TE} = & \sum_{m=1}^M E_{inc}^{TE} \cos \psi_m e^{jk_0 z \sin \psi_m} \\ & \left[ \sum_{n=-\infty}^{n=\infty} (-j)^n [C_n H_n^{(1)}(k_0 r \cos \psi_m) \frac{(-n \sin \psi_m)}{k_0 r \cos^2 \psi_m} + \right. \\ & \left. \frac{j}{\cos \psi_m} C_n^{TE} H_n^{(1)'}(k_0 r \cos \psi_m)] e^{jn\phi} \hat{a}_\phi \right. \\ & \left. + \sum_{n=-\infty}^{n=\infty} (-j)^n C_n H_n^{(1)}(k_0 r \cos \psi_m) e^{jn\phi} \hat{a}_z \right] \end{aligned} \quad (3.44)$$

Similarly, total far electromagnetic scattered field by the sandwich radome seam with incident radiation for the transverse magnetic case is found as:

$$E_z^{sTM} = \sum_{m=1}^M E_{inc}^{TM} \cos \psi_m e^{jk_0 z \sin \psi_m} \sum_{n=-\infty}^{n=\infty} (-j)^n C_n^{TM} H_n^{(1)}(k_0 r \cos \psi_m) e^{jn\phi} \quad (3.45)$$

$$\begin{aligned}
E_{\phi}^{sTM} = & \sum_{m=1}^M E_{inc}^{TM} \cos \psi_m e^{jk_0 z \sin \psi_m} \\
& \sum_{n=-\infty}^{n=\infty} (-j)^n [C_n^{TM} H_n^{(1)}(k_0 r \cos \psi_m) \frac{(-n \sin \psi_m)}{k_0 r \cos^2 \psi_m} \\
& - \frac{j}{\cos \psi_m} \sqrt{\frac{\mu_0}{\epsilon_0}} C_n H_n^{(1)'}(k_0 r \cos \psi_m)] e^{jn\phi'}
\end{aligned} \quad (3.46)$$

where  $C_n^{TM}$  is expressed as the following:

$$C_n^{TM} = -\frac{V_n P_n - q_n^2 J_n(x_0) H_n^{(1)}(x_0)}{P_n N_n - [q_n H_n^{(1)}(x_0)]^2} \quad (3.47) \quad \text{with,}$$

$$V_n = J_n(x_0) - Z_n J_n'(x_0) \quad (3.48)$$

Finally, scattered transverse magnetic field of the antenna and M arbitrary distributed sandwich radome structure is found to be:

$$\begin{aligned}
\vec{E}^{sTM} = & \sum_{m=1}^M E_{inc}^{TM} \cos \psi_m e^{jk_0 z \sin \psi_m} \\
& \sum_{n=-\infty}^{n=\infty} (-j)^n C_n^{TM} H_n^{(1)}(k_0 r \cos \psi_m) e^{jn\phi'} \hat{a}_z \\
& + \sum_{m=1}^M E_{inc}^{TM} \cos \psi_m e^{jk_0 z \sin \psi_m} \\
& \sum_{n=-\infty}^{n=\infty} (-j)^n [C_n^{TM} H_n^{(1)}(k_0 r \cos \psi_m) \frac{-n \sin \psi_m}{k_0 r \cos^2 \psi_m} \\
& - \frac{j}{\cos \psi_m} \sqrt{\frac{\mu_0}{\epsilon_0}} C_n H_n^{(1)'}(k_0 r \cos \psi_m)] e^{jn\phi'} \hat{a}_\phi
\end{aligned}
\tag{3.49}$$

Pyramidal horn type antenna which has aperture on the x-y plane with the aperture dimensions a and b has far electromagnetic field for  $TE_{10}$  (the dominant field) is expressed [17] as given in Appendix:

$$\begin{aligned}
\vec{E}_{ANTENNA} = & \frac{jk_0}{R} E_0 a b e^{-jk_0 R} \left[ \left\{ \sin \phi \frac{\sin(k_0 \sin \theta \sin \phi \frac{b}{2})}{k_0 \sin \theta \sin \phi \frac{b}{2}} \right\} \right. \\
& \left. \left[ \frac{\cos(k_0 \sin \theta \cos \phi \frac{a}{2})}{\pi^2 - 4(k_0 \sin \theta \cos \phi \frac{a}{2})^2} \right] \hat{a}_\theta + \right. \\
& \left. \left( \cos \phi \frac{\sin(k_0 \sin \theta \sin \phi \frac{b}{2})}{k_0 \sin \theta \sin \phi \frac{b}{2}} \right) \left[ \frac{\cos(k_0 \sin \theta \cos \phi \frac{a}{2})}{\pi^2 - 4(k_0 \sin \theta \cos \phi \frac{a}{2})^2} \right] \hat{a}_\phi \right]
\end{aligned}
\tag{3.50}$$

where  $a$  and  $b$  is the aperture dimensions,  $k_0$  is the wave number.

Scattering from the sandwich radome structure is expressed in cylindrical coordinates. For a final solution the far electromagnetic field of the scattered field should be expressed in spherical coordinates to have vector summation of the antenna original field and scattered field by the sandwich radome seams.

To express the scattered field in spherical coordinates, defined distances and coefficients should be transformed such as:

$$r = R \sin \theta \quad (3.51)$$

$$\phi = \phi \quad (3.52)$$

$$z = R \cos \theta \quad (3.53)$$

$$\begin{bmatrix} A_r \\ A_\theta \\ A_\phi \end{bmatrix} = \begin{bmatrix} \sin \theta & 0 & \cos \theta \\ \cos \theta & 0 & -\sin \theta \\ 0 & 1 & 0 \end{bmatrix} \begin{bmatrix} A_r \\ A_\phi \\ A_z \end{bmatrix} \quad (3.54)$$

Then, found  $\vec{E}_{Scattered}^{TE}$  is expressed in spherical coordinates as:

$$\begin{aligned}
& \sum_{m=1}^M E_{inc}^{TE} \cos \psi_m e^{jk_0 R \cos \theta \sin \psi_m} \\
& \left[ \sum_{n=-\infty}^{n=\infty} (-j)^n C_n H_n^{(1)}(k_0 R \sin \theta \cos \psi_m) e^{jn\phi} (-\sin \theta) \hat{a}_\theta \right] \\
& + \left[ \sum_{n=-\infty}^{n=\infty} (-j)^n [C_n H_n^{(1)}(k_0 R \sin \theta \cos \psi_m) \right. \\
& \left. \frac{(-n \sin \psi_m)}{k_0 R \sin \theta \cos^2 \psi_m} + \frac{j}{\cos \psi_m} C_n^{TE} H_n^{(1)'}(k_0 R \sin \theta \cos \psi_m)] e^{jn\phi} \hat{a}_\phi \right]
\end{aligned}
\tag{3.55}$$

Finally,  $\vec{E}_{Total}$  which is the total far electromagnetic field of the antenna and sandwich radome structure is found as given in equation (3.27).  $\vec{E}_{Total}$  is equal to:

$$\begin{aligned}
\vec{E}_{Total} = & \sum_{m=1}^M \sqrt{\frac{\eta_0 P_{21,6} f a}{4\pi}} \frac{1}{u_m} \cos \psi_m e^{jk_0 R \cos \theta \sin \psi_m} \\
& \left[ \sum_{n=-\infty}^{n=\infty} (-j)^n C_n H_n^{(1)}(k_0 R \sin \theta \cos \psi_m) e^{jn\phi} (-\sin \theta) \right] + \\
& \frac{jk_0}{R} E_0 a b e^{-jk_0 R} \left[ \sin \phi \frac{\sin(k_0 \sin \theta \sin \phi \frac{b}{2})}{k_0 \sin \theta \sin \phi \frac{b}{2}} \right] \\
& \left[ \frac{\cos(k_0 \sin \theta \cos \phi \frac{a}{2})}{\pi^2 - 4(k_0 \sin \theta \cos \phi \frac{a}{2})^2} \right] \widehat{a}_\theta \\
& + \left[ \sum_{n=-\infty}^{n=\infty} (-j)^n [C_n H_n^{(1)}(k_0 R \sin \theta \cos \psi_m) \frac{(-n \sin \psi_m)}{k_0 R \sin \theta \cos^2 \psi_m} \right. \\
& \left. + \frac{j}{\cos \psi_m} C_n^{TE} H_n^{(1)'}(k_0 R \sin \theta \cos \psi_m)] e^{jn\phi} \right] \\
& + \frac{jk_0}{R} E_0 a b e^{-jk_0 R} \left( \cos \phi \frac{\sin(k_0 \sin \theta \sin \phi \frac{b}{2})}{k_0 \sin \theta \sin \phi \frac{b}{2}} \right) \\
& \left[ \frac{\cos(k_0 \sin \theta \cos \phi \frac{a}{2})}{\pi^2 - 4(k_0 \sin \theta \cos \phi \frac{a}{2})^2} \right] \widehat{a}_\phi
\end{aligned}
\tag{3.56}$$

Note that total field is expressed as the summation of the antenna far electromagnetic field for the dominant mode ( $TE_{10}$ ) and the total scattered field with this mode accordingly. Also note that,  $u_m$  in the final equation represents the distance between the  $m^{th}$  sandwich radome seam and the



aperture of the antenna. The effect of this distance on the electromagnetic field pattern is discussed in the following section via the simulations.

### 3.4 Simulations Based on the Analysis

This section is devoted to the simulations based on the electromagnetic scattering analysis of the sandwich radome seams in this chapter. Antenna original far electromagnetic field is compared with the total far electromagnetic field which is the combination of antenna original far electromagnetic field and the scattered electromagnetic field of arbitrary distributed sandwich radome seam structure.

At resonant frequency of 1 GHz with the dimensions of  $a = 76,2 \text{ cm} (2,54\lambda)$  and  $b = 55,9 \text{ cm} (1,86\lambda)$  with 1 kw input power, first the horn antenna far electromagnetic field characteristics for the dominant mode( $TE_{10}$ ) is obtained. Then, the far electromagnetic field pattern characteristics of horizontal cylinder ( $\psi = 0$ ) with the distance from the aperture of horn antenna as  $6\lambda (u = 6\lambda)$  is obtained. As a realistic approach the coated cylinder diameter is taken as  $a_0 = 6 \text{ cm}$  and  $a_1 = 1 \text{ cm}$ . Finally, far electromagnetic field pattern characteristics for 7 seam structures ( $M=7$ ) with the angle of inclination  $\psi_m = 30^\circ$  for  $m=1,2,3,4,5,6$  and  $\psi_m = 0^\circ$  for  $m=7$ , assuming the same distance ( $u_m = 6\lambda$ ) from the aperture centre is obtained.

The graph presented in Figure 20 contains all three E-Field pattern characteristics expressed above. The characteristics shown in blue color is the horn antenna original total far E-Field pattern characteristics. The

characteristic in green color shows the combination of scattered E-Field of single horizontal dielectric coated cylinder which is placed at  $u = 6\lambda$  distance from the aperture and the horn antenna original total far E-Field characteristics. Finally the characteristic in red color shows the total E-Field pattern characteristics of horn antenna and 7 seam structures with the angle of inclination  $\psi_m = 30^\circ$  for  $m=1,2,3,4,5,6$  and  $\psi_m = 0^\circ$  for  $m=7$ , assuming  $u_m = 6\lambda$  distance from the aperture centre. As it can be observed from the graphs the seam structures lead to distortions on the original antenna field characteristics as the number of seam structures increases. New side lobes are generated with various levels and directions. This is clearly presented with multi numbered sandwich radome seam distribution. Typically these are the effects of scattering electromagnetic fields of the seams in the near field of the antenna.

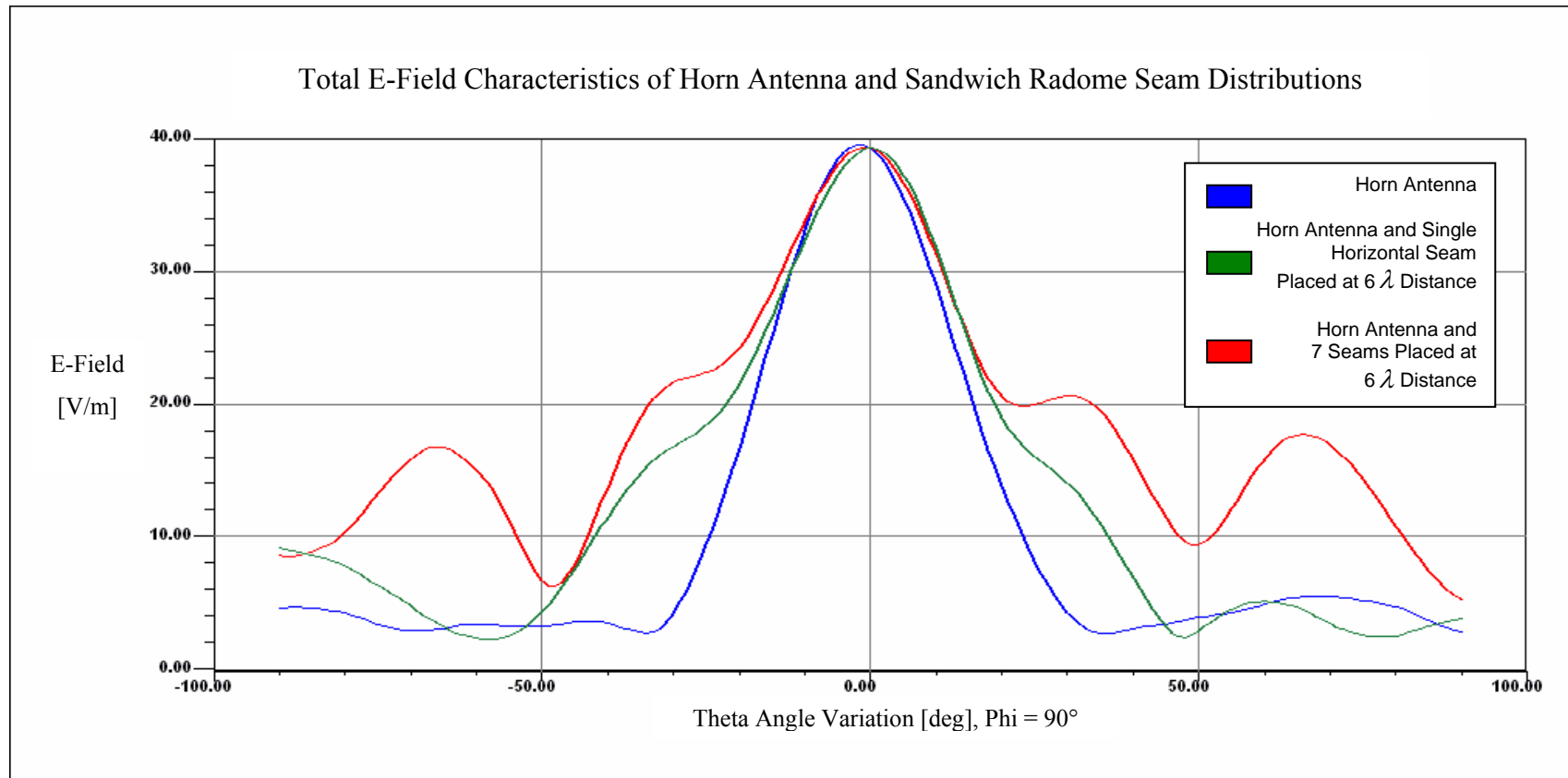


Figure 20- Far E-Field Characteristics of Antenna and Different Sandwich Radome Seam Distributions

After having far electromagnetic field pattern characteristics of the analysis done in Section 3.1, 3.2 and 3.3., same structures are designed and simulated with RF Software program HFSS™ with various sandwich radome seam distributions to improve the perspective of the simulation environment. In the designs, a horn antenna is designed with the aperture dimensions of 76.2 cm and 55.9 cm, the funnel length of 157.4 cm and with the base dimensions of 9.05 cm, 11.4 cm and 25.86 cm at the resonant frequency of 1 GHz with perfect electric conductor material in HFSS™. The design of the horn antenna is presented in Figure 21.

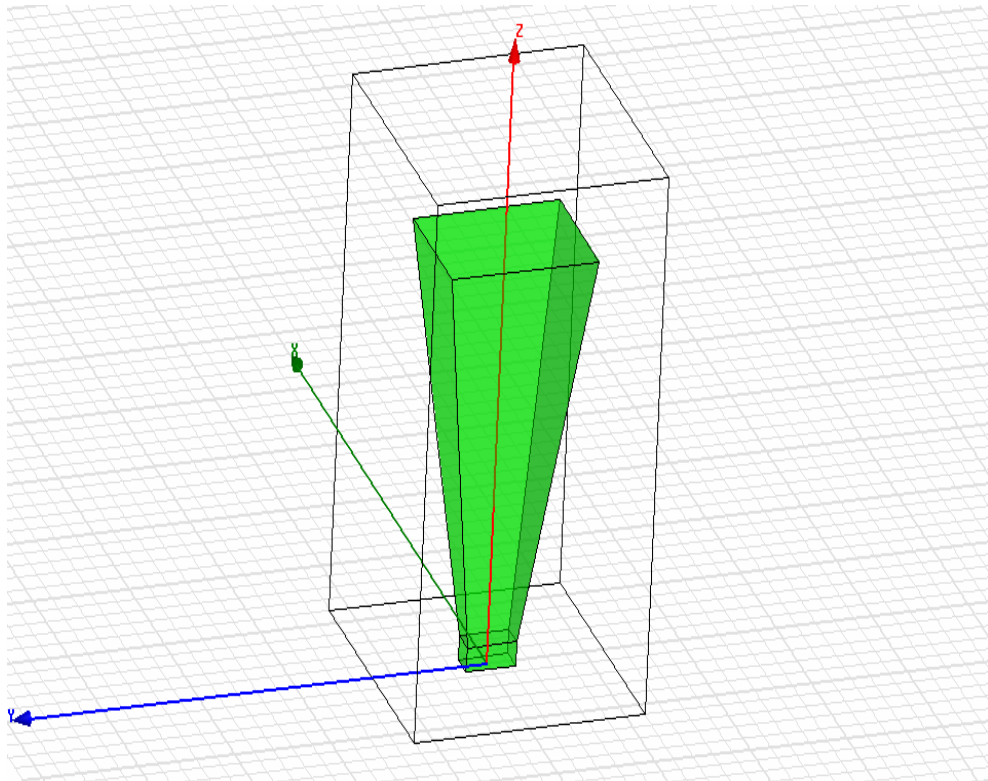


Figure 21- Design of Pyramidal Horn Antenna

Before inserting the sandwich radome seams in the near field of the horn antenna, original antenna field pattern characteristics is obtained to observe the effect of the scattering effect of the sandwich radome seams on the total far electromagnetic field pattern. The designed horn antenna's original 3D Polar E-Field Pattern Characteristics is given in Figure 22.

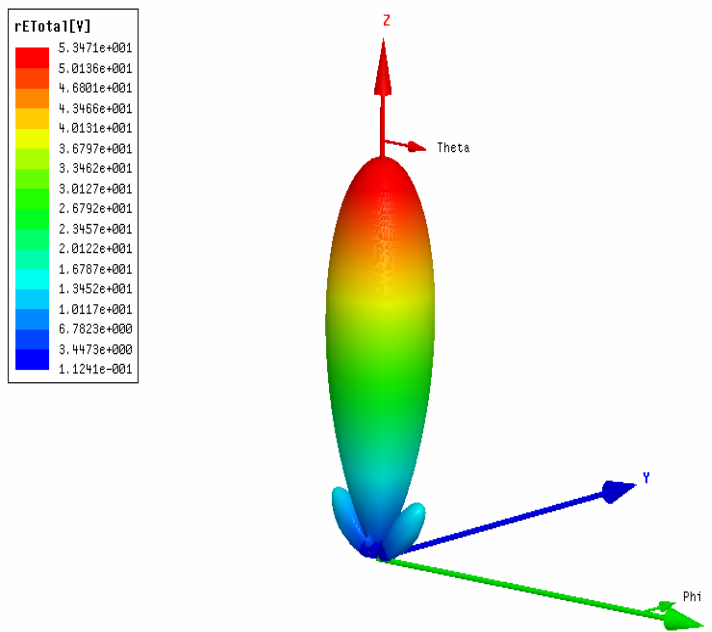


Figure 22 – 3D Polar Plot of the Horn Antenna E-Field Pattern

The following 3D Rectangular E-Field pattern is obtained as in Figure 23. This figure clearly shows the level of side lobes on the  $\phi$  plane.

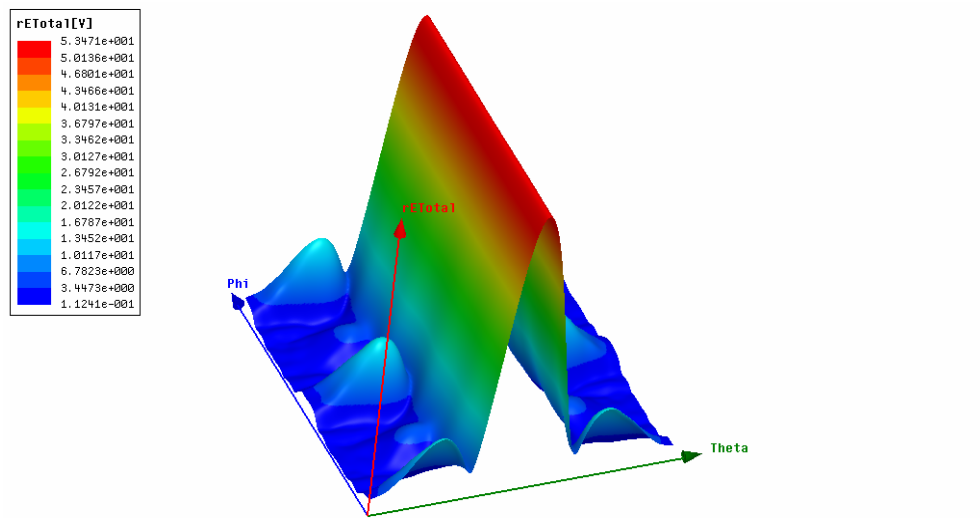


Figure 23 - 3D Rectangular Plot of the Antenna E-Field Pattern

Figure 24 represents antenna's 2D total E-Field radiation characteristics on the principal planes.

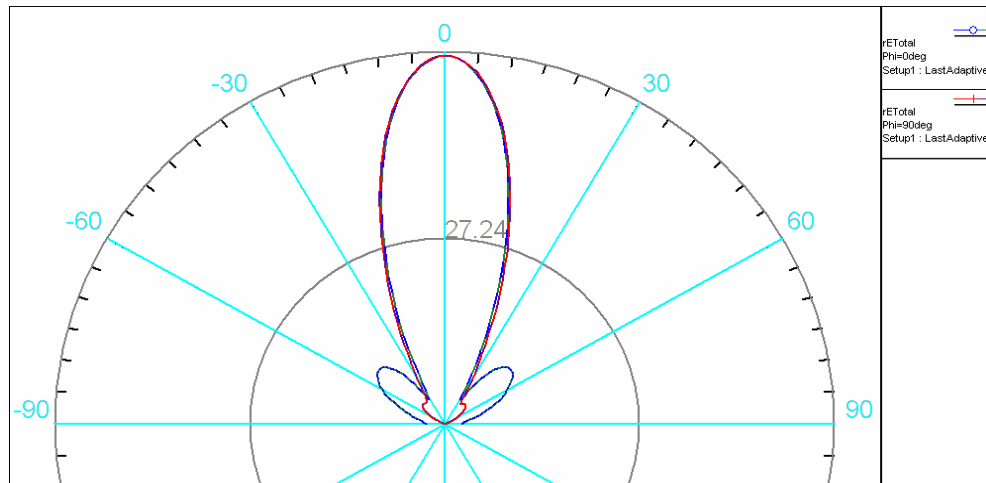


Figure 24- 2D Total E-Field Radiation Characteristics of the Antenna on Principal Planes

In Figure 24 red line represents the E-plane ( $\phi = \pi / 2$ ) characteristics and blue line represents H-plane ( $\phi = 0$ ) characteristics. As seen in the figure side lobes are in the H-plane ( $\phi = 0$ ). Major lobe has the same pattern characteristics both for the E-plane ( $\phi = \pi / 2$ ) and H-plane ( $\phi = 0$ ).

After having the original antenna far electromagnetic field pattern characteristics, the next step is the obtaining the total far electromagnetic field characteristics which is the combination of original antenna electromagnetic field and scattering field of sandwich radome seams. The step of obtaining the total far electromagnetic field pattern characteristics of the antenna and sandwich radome seams is partitioned into subsets to examine scattering effect of the seams on the original antenna field clearly. These subsets are inserting single horizontal sandwich radome seam, cross-examining scattering effect of the seam polarization with respect to the antenna aperture by changing the polarization of the sandwich radome seam and finally finding the total far electromagnetic E-Field pattern characteristics of arbitrary distributed sandwich radome seams and the antenna.

To examine the effect of the first subset in HFSS™ with the previously designed horn antenna, following geometry is constituted as presented in Figure 25. Horizontal dielectric seam which is made of Silicon Dioxide with the dimensions as  $4,8 \lambda$  length and  $0,2 \lambda$  diameter is placed at a distance of  $6 \lambda$  from the aperture as shown in figure.

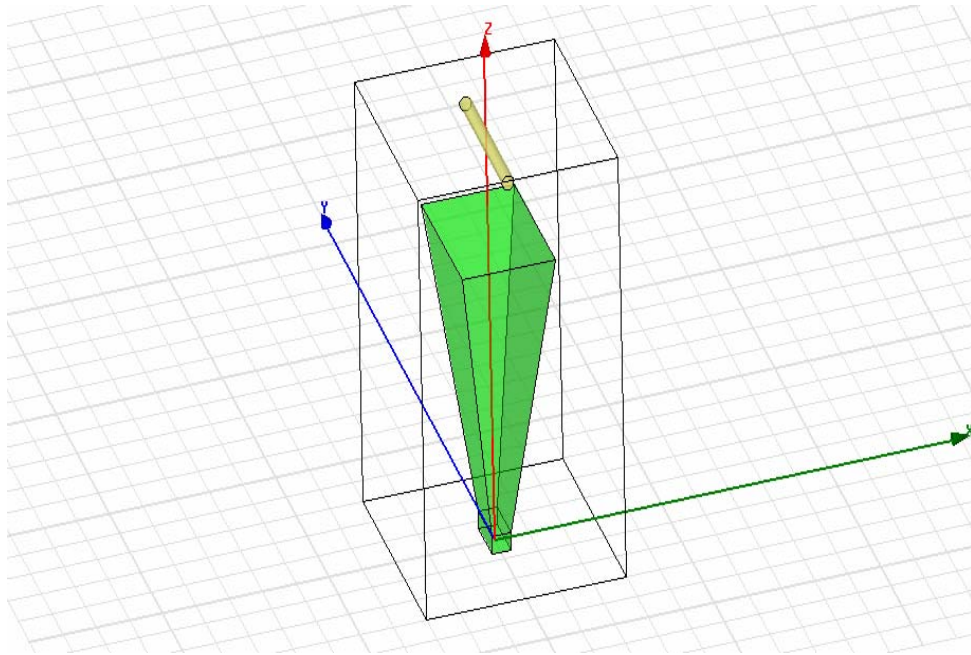


Figure 25- Placement of  $4,8 \lambda$  Length and  $0,2 \lambda$  Diameter Horizontal Sandwich Radome Seam at  $6\lambda$  Distance to the Horn Antenna

With this geometry, 3D Polar E-Field pattern in Figure 26 is obtained. With the effect of scattering from the seam structure there are newly generated side lobes in the field pattern while compared with the pure horn antenna polar E- Field Pattern given in Figure 22.



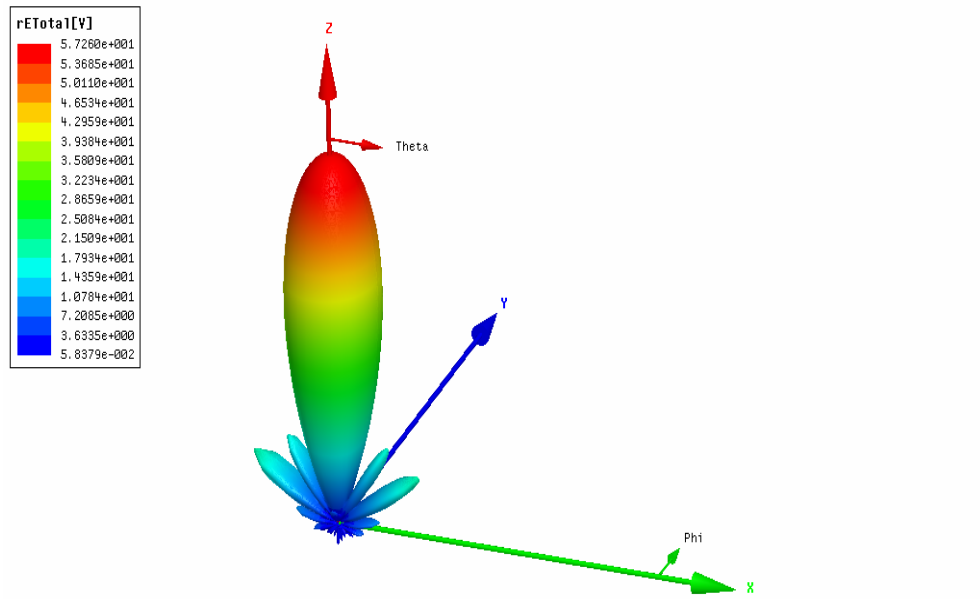


Figure 26 - 3D Polar Plot of the Total E-Field Pattern of the  $4.8 \lambda$  Length and  $0.2 \lambda$  Diameter Horizontal Sandwich Radome Seam Placed at  $6\lambda$  Distance to the Antenna

To present the effect of scattering on the side lobes, following 3D Rectangular E-Field Pattern characteristic is obtained as given in Figure 27. It is observed that the seam leads to increase the side lobe levels and newly generated side lobes are occurred in the total far electromagnetic E-field pattern characteristics.

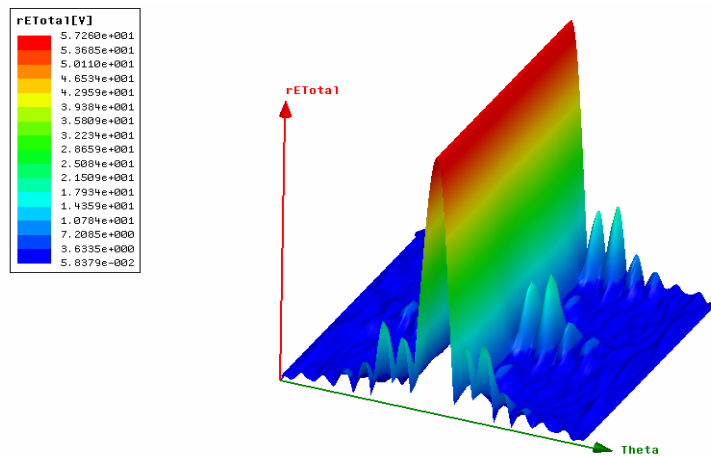


Figure 27 - 3D Rectangular Plot E-Field Pattern of the  $4,8 \lambda$  Length and  $0,2 \lambda$  Diameter Horizontal Sandwich Radome Seam Placed at  $6\lambda$  Distance to the Antenna

Figure 28 represents 2D Total E-Field radiation characteristics of the horn antenna and horizontal sandwich radome seam on the principal planes.

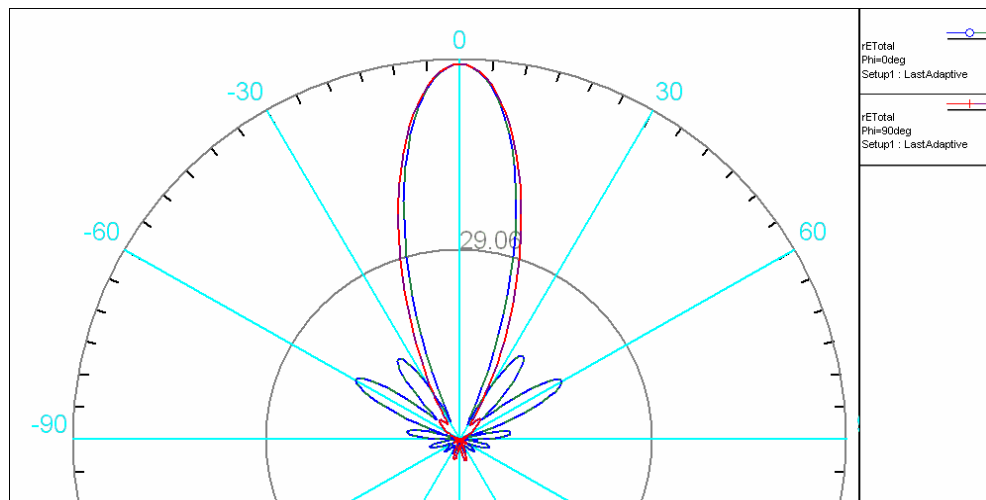


Figure 28 - 2D Total E-Field Radiation Characteristics of  $4,8 \lambda$  Length and  $0,2 \lambda$  Diameter Horizontal Sandwich Radome Seam Placed at  $6\lambda$  Distance to the Antenna

In Figure 28 red line represents the E-plane ( $\phi = \pi / 2$ ) characteristics and blue line represents H-plane ( $\phi = 0$ ) characteristics of total electric field. As seen in the figure newly generated side lobes are occurred on the H-plane ( $\phi = 0$ ) with the effect of horizontal sandwich radome seam in the near field of the horn antenna.

The next analysis is related with the effect of the polarization of the sandwich radome seam on the total far electromagnetic field characteristics. To analyse this effect following design in HFSS™ is constructed as presented in Figure 29.  $4,8 \lambda$  Length and  $0,2 \lambda$  Diameter dielectric seam structure is placed on the perpendicular direction in front of the antenna as presented in the figure. The nearest distance between the cylinder and the antenna aperture is kept  $6\lambda$  as in the horizontal sandwich radome seam distribution case.

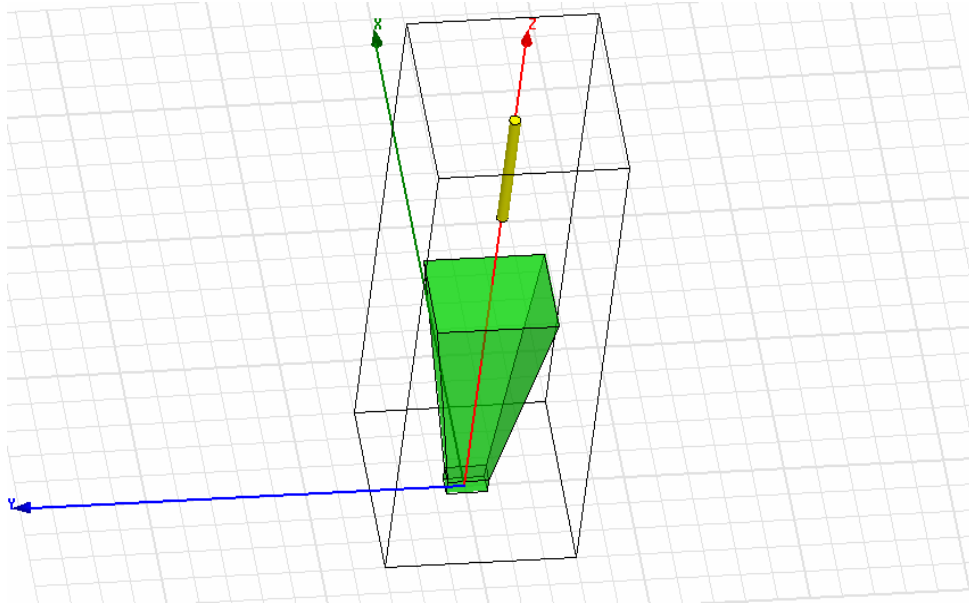


Figure 29- Placement of  $4,8 \lambda$  Length and  $0,2 \lambda$  Diameter Perpendicular Sandwich Radome Seam at  $6\lambda$  Distance to the Antenna

With this distribution of the dielectric seam in the near field of the antenna following far electromagnetic field pattern characteristics are obtained in Figure 30, Figure 31 and Figure 32.

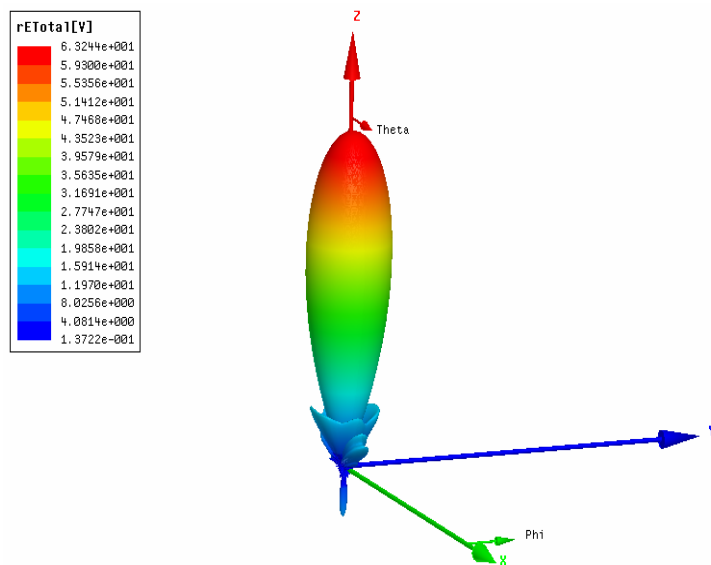


Figure 30 - 3D Polar Plot of the E-Field Pattern with  $4.8 \lambda$  Length and  $0.2 \lambda$  Diameter Perpendicular Sandwich Radome Seam in the Near Field of the Antenna

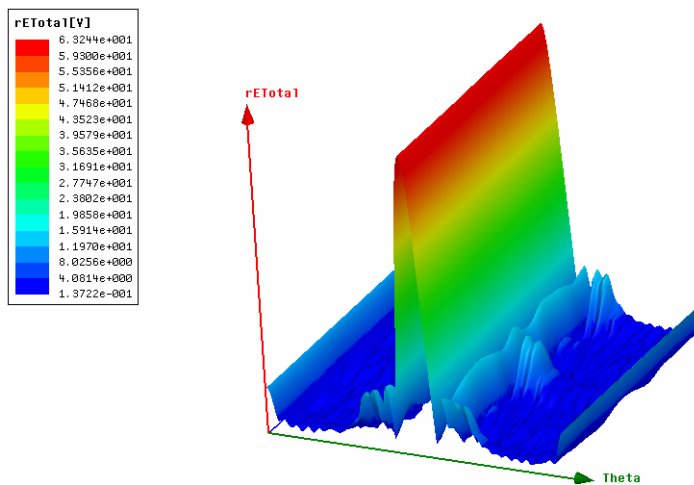


Figure 31 - 3D Rectangular Plot of the E-Field Pattern of the  $4,8 \lambda$  Length and  $0,2 \lambda$  Diameter Perpendicular Sandwich Radome Seam and the Antenna

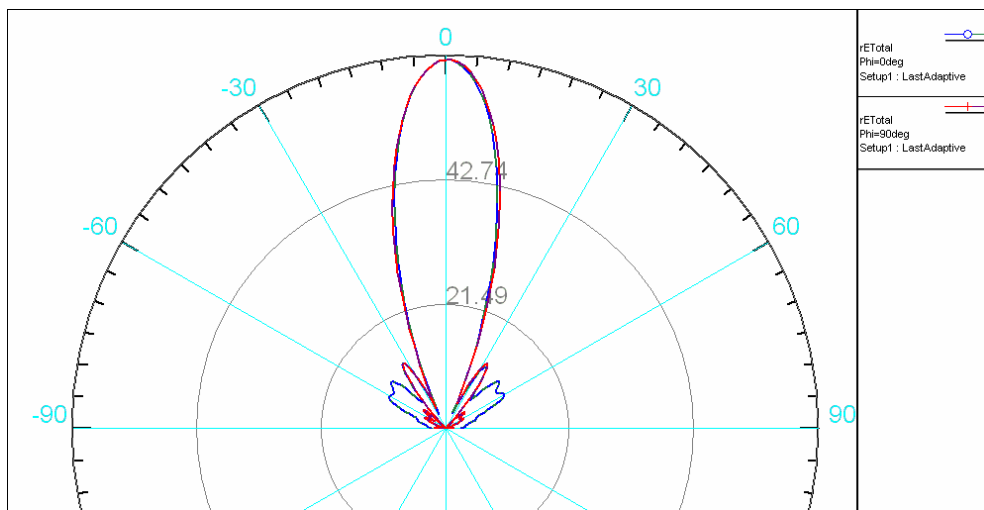


Figure 32- 2D Total E-Field Radiation Characteristics of  $4,8 \lambda$  Length and  $0,2 \lambda$  Diameter Perpendicular Sandwich Radome Seam Placed at  $6\lambda$  Distance to the Antenna

Figure 32 shows 2D radiation pattern characteristics of perpendicular sandwich radome seam and the horn antenna. In this figure red line represents the E-plane ( $\phi = \pi / 2$ ) characteristics and blue line represents H-plane ( $\phi = 0$ ) characteristics of total electric field.

As presented in Figures 30, 31 and 32, scattering effect of dielectric perpendicular seam and the antenna is lower when compared with the characteristics of antenna and dielectric horizontal sandwich radome seam geometry in Figures 26, 27 and 28. This phenomenon can be explained as the blocking area degradation of the aperture in the near field when it is placed in perpendicular polarization on to the aperture plane. Actually, it is an expected result of the analysis done in Section 3.2. Since the incidence angle is  $\psi = 90^\circ$  for perpendicular directed seam in front of the antenna,  $\cos\psi$  expression in the  $\vec{E}_{Scattered}^{TE}$  equation leads to zero in the scattered electromagnetic field expression. Therefore, far electromagnetic field pattern is constituted directly from the antenna original field with this distribution.

Finally, placement of 7 sandwich radome seams which have dimensions as  $4,8 \lambda$  length and  $0,2 \lambda$  diameter is simulated. The angle of inclination of the sandwich radome seams are taken  $\psi = 30^\circ$  for 6 seams and  $\psi = 0^\circ$  for the horizontal seam such that the other 6 seams are attached the horizontal sandwich radome seam. The distances from the aperture are taken as  $6\lambda$  as in the previous simulations.

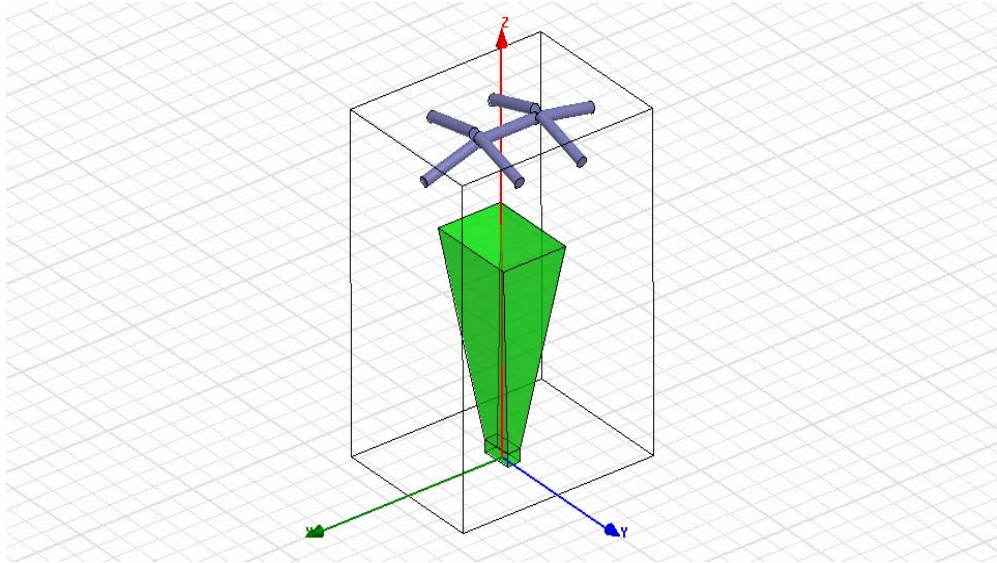


Figure 33- Multi Numbered Distribution of  $4,8 \lambda$  Length and  $0,2 \lambda$  Diameter Sandwich Radome Seams Placed at  $6\lambda$  Distance to the Antenna

Figure 33 presents multi numbered seam distribution defined in the above paragraph. As clearly presented in the figure, the distribution of sandwich radome seams constitutes a typical framework of a sandwich type radome.

With this design of antenna and sandwich radome seams, following total far electromagnetic E-Field pattern characteristics are obtained as given in Figure 34 and Figure 35.

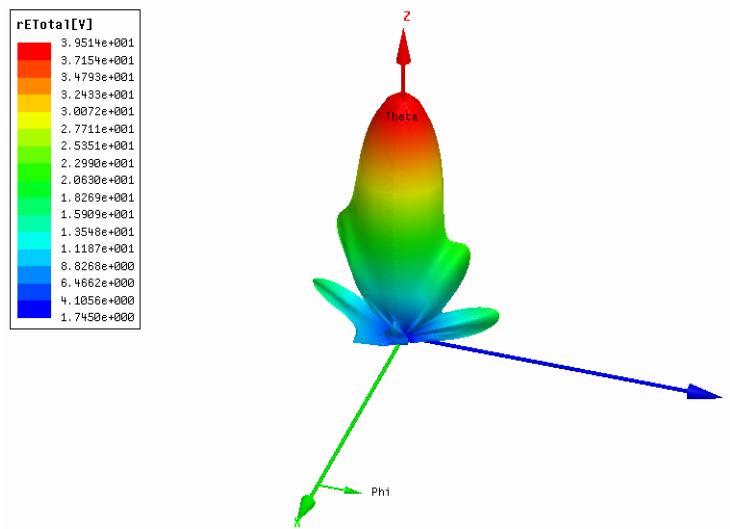


Figure 34 - 3D Polar Plot of the E-Field of the Distributed  $4.8 \lambda$  Length and  $0.2 \lambda$  Diameter Sandwich Radome Seams Placed at  $6\lambda$  Distance to the Antenna

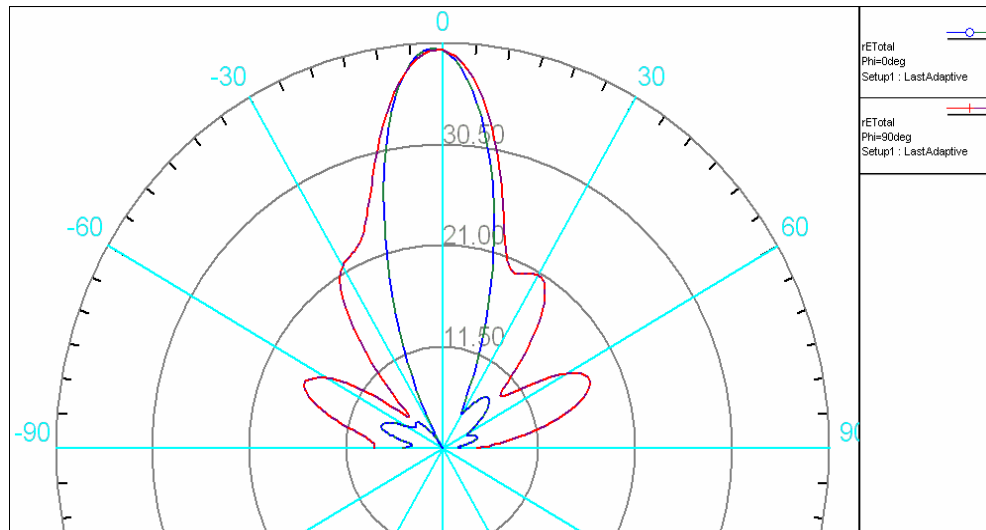


Figure 35 - 2D Total E-Field Radiation Characteristics of Distributed  $4.8 \lambda$  Length and  $0.2 \lambda$  Diameter Sandwich Radome Seams Placed at  $6\lambda$  Distance to the Antenna



Figure 35 represents 2D Total E-Field radiation characteristics of distributed sandwich radome seams and the antenna. In this figure red line represents the E-plane ( $\phi = \pi/2$ ) characteristics and blue line represents H-plane ( $\phi = 0$ ) characteristics of total electric field. Distortion of field pattern characteristics on both planes is clearly presented in this figure.

Figure 34 and Figure 35 show that there are newly generated high powered side lobes occurred in the field pattern with the effect of distributed sandwich radome seams in the near field of the antenna. This HFSS<sup>TM</sup> result is well adjusted with the analysis done in section 3.3. This resemblance is shown in Figure 20 and Figure 35. In both figures, result of the placement of 7 sandwich radome seams which have dimensions as  $4,8 \lambda$  length and  $0,2 \lambda$  diameter such that the angle of inclination of the incident antenna field to the sandwich radome seams is taken  $\psi = 30^\circ$  for 6 seams and  $\psi = 0^\circ$  for the horizontal seam at  $6\lambda$  distances from the aperture is presented. As seen from the characteristics obtained in Figures 20, 34 and 35 distributed sandwich radome seams change the shape of the main beam of the antenna original field in the pattern and lead high powered side lobes on the E-plane especially for the angles  $\theta = 30^\circ$  and  $\theta = 70^\circ$  respectively.

To sum up, multi numbered sandwich radome seams positioned in the near field of the antenna leads to important distortion on the antenna original field pattern as expected. In Chapter 4, ways to decrease the distortion via the effect of the sandwich radome framework structure is discussed and two different design methods are proposed to solve the problem.

# **CHAPTER 4**

## **ENHANCING ELECTROMAGNETIC TRANSPARENCY OF SANDWICH TYPE RADOMES**

### **4.1 Factors Effecting Electromagnetic Performance of the Structure**

Radomes are very crucial to protect the antennas from harsh weather conditions and to sustain the operational performance of these systems for a long period of time. However, if the radomes are not appropriately designed, they lead important distortions on the original antenna signal. This chapter is totally devoted to discuss the ways of enhancing electromagnetic performance of the antenna and sandwich type radome systems.

As mentioned before, panels of the sandwich radome systems are technologically fabricated using honeycomb polyurethane materials such that insertion loss due to panels in sandwich radomes is much less than 0,1 dB. However, the seams that connect these electromagnetically transparent panels lead 4 to 100 times greater insertion and scattering losses when compared with the panels. This is the reason of devoting this thesis work on

analyzing and enhancing electromagnetic transparency of the sandwich radome flange framework.

Enhancing electromagnetic transparency methods of sandwich radomes can be grouped in two different parts. The first group is the arranging the geometric positions of the sandwich radome seams. The next one is adding conducting materials in the dielectric seams to decrease the capacitance of the structure by tuning.

## **4.2 Importance of the Distance of the Seam Structure to the Antenna Aperture**

Seam blocking effect increases in the near field when the distance between the aperture and the seam structure decreases. This blocking leads high levels of scattering on the incident electromagnetic field generated by the antenna. Level of scattering effect by changing the distance of the seam from the aperture is analyzed by the following simulation in HFSS™.  $4,8\lambda$  length and  $0,2\lambda$  diameter sandwich radome seam material made of silicon dioxide is placed in front of the aperture of the antenna with different distances. First one is placed at a  $3\lambda$  wavelength distance and the other one is placed at a  $10.7\lambda$  wavelength distance from the aperture. The Figure 36 shows the placement of horizontal dielectric seam in the near field of the antenna at a distance of  $3\lambda$  from the aperture. The Figure 37 presents the placement of same horizontal dielectric seam at a distance of  $10.7\lambda$  from the aperture of the antenna.

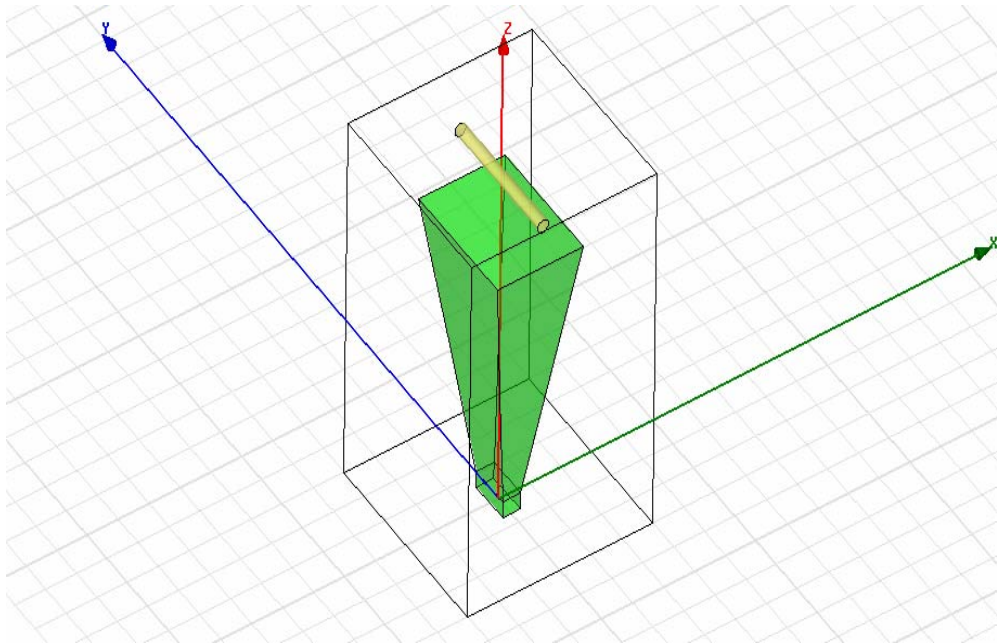


Figure 36 -  $4,8 \lambda$  Length and  $0,2 \lambda$  Diameter Sandwich Radome Seam  
Placed at  $3 \lambda$  Distance to the Aperture

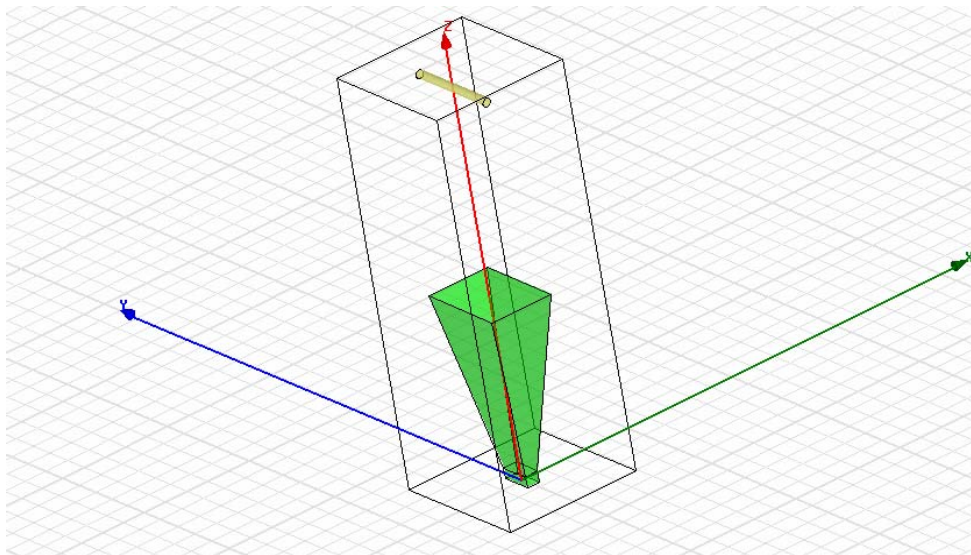


Figure 37 -  $4,8 \lambda$  Length and  $0,2 \lambda$  Diameter Sandwich Radome Seam  
Placed at  $10.7\lambda$  Distance to the Aperture

Far electromagnetic field distance from the antenna where the Fraunhofer region starts can be calculated with:

$$D = \frac{2d^2}{\lambda} \quad (4.1)$$

where  $D$  is the minimum far electromagnetic field distance from the antenna aperture,  $d$  is the aperture hypotenuse and  $\lambda$  is the wavelength. Frequency of the antenna is 1 GHz, the aperture dimensions are 76.2 and 55.9 cm respectively as in the previous analyzes. From the equation the distance  $D$  is around  $18\lambda$ . Therefore, 10.7 wavelength distant sandwich radome seam is in Fresnel region as a realistic case.

Following 3D Rectangular E-Field characteristics is obtained with the horizontal placement of  $3\lambda$  wavelength distant sandwich radome seam in front of the aperture as presented in Figure 38. Figure 39 shows total E-field pattern characteristics of horizontally placed  $10.7\lambda$  distant sandwich radome seam. Figure 40 shows the total polar E-Field plot of  $3\lambda$  distant sandwich radome seam in front of the aperture. Figure 41 shows the total polar E-Field plot  $10.7$  wavelength distant sandwich radome seam in front of the aperture.

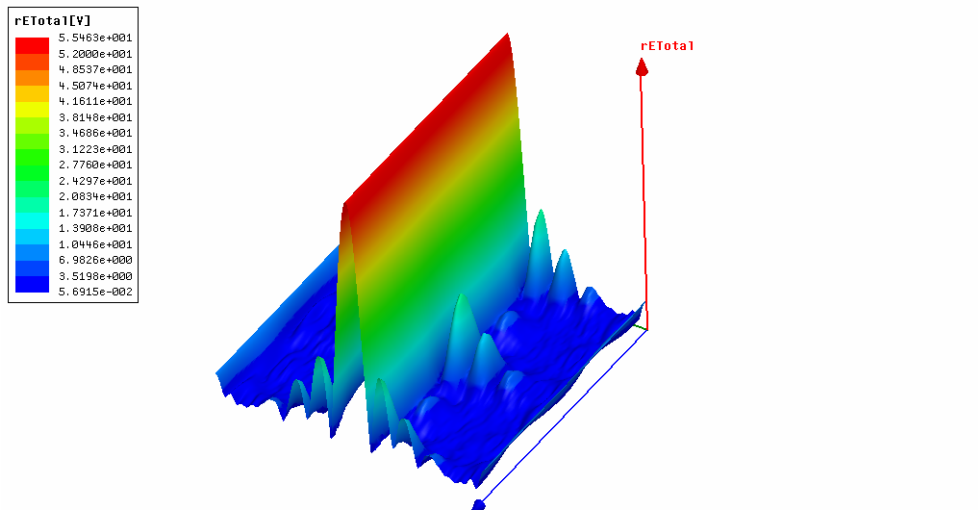


Figure 38 - 3D Cartesian Plot of the Total E-Field Pattern of  $3\lambda$  Distant  $4,8\lambda$  Length and  $0,2\lambda$  Diameter Sandwich Radome Seam

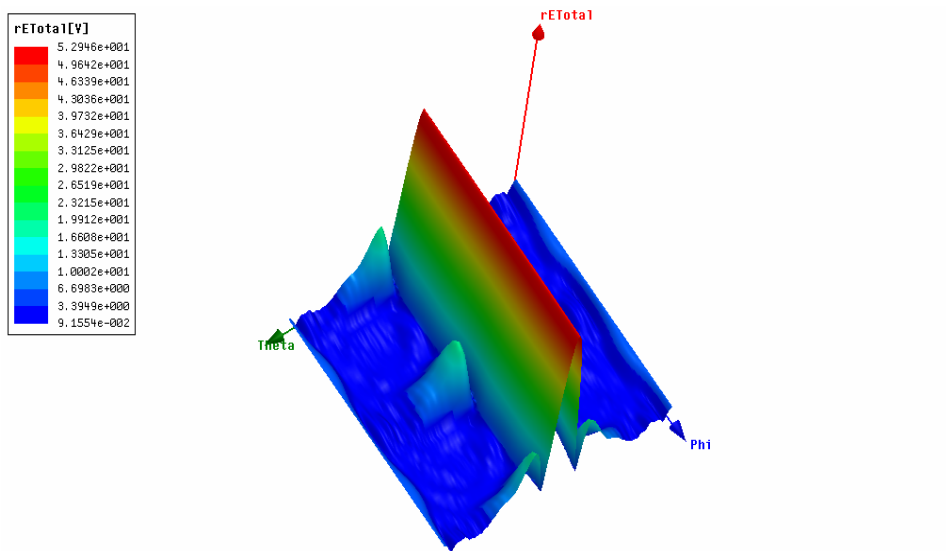


Figure 39 - 3D Cartesian Plot of the Total E-Field Pattern of  $10.7\lambda$  Distant  $4,8\lambda$  Length and  $0,2\lambda$  Diameter Sandwich Radome Seam

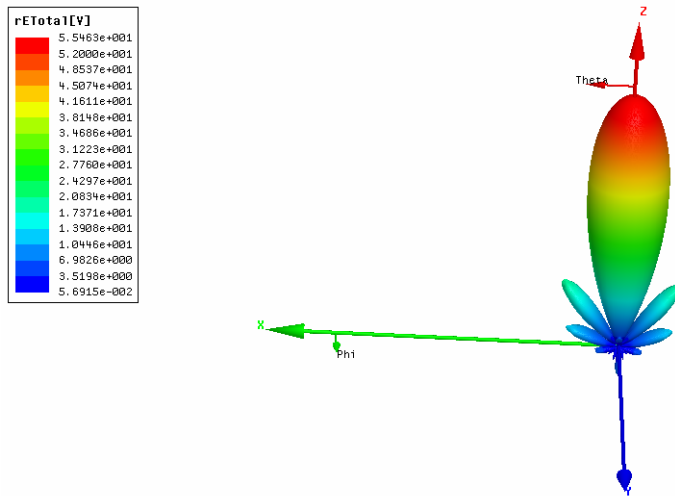


Figure 40 - Polar Plot of the Total E-Field Pattern of  $3\lambda$  Distant  $4,8 \lambda$  Length and  $0,2 \lambda$  Diameter Sandwich Radome Seam

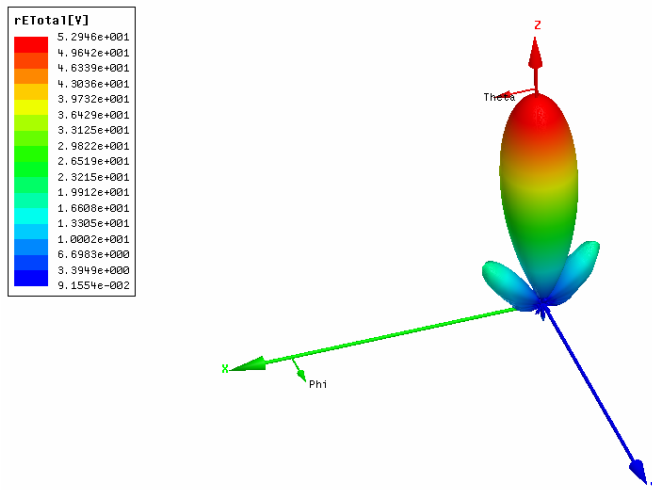


Figure 41 - Polar Plot of the Total E-Field Pattern of  $10.7\lambda$  Distant  $4,8 \lambda$  Length and  $0,2 \lambda$  Diameter Sandwich Radome Seam

It should be noted that scattering effect with near sandwich radome seam is higher than the far sandwich radome seam as expected. Design with  $3\lambda$  distant sandwich radome seam has newly generated side lobes which are formed by the scattering effect of sandwich radome seam as given in Figures 38 and 40. However, the design with  $10.7\lambda$  distant sandwich radome seam has no newly generated side lobes and the pattern is quite similar to the original antenna field pattern characteristics as given in Figures 39 and 41. Therefore, the design of sandwich radome seams should be such that the distance of the seams from the aperture of the antenna should be kept as far as possible. However, it should always be kept in mind that this means a larger area for the antenna system, higher cost for production and installation. Having these constraints the distance of the seams from the aperture should be designed such that the effect of scattering could be adoptable.

### **4.3 Enhancing Electromagnetic Transparency by Quasi-Random Geometric Distribution of Seams**

In the section 4.2, the effect of the distance of the sandwich radome seam on the electromagnetic transparency of the structure is expressed. In this section a way of enhancing electromagnetic transparency without changing the distance of the seams from the antenna structure is presented. This design method is called Geometric Randomization. It is also known as quasi-random geometric distribution of seams [12]. Enhancing electromagnetic transparency can be obtained by minimizing the total scattered field which is composed of the scattered field of each sandwich radome seam forming the whole framework of the sandwich radome. As analyzed in previous chapter total scattered field is the vector summation of



the scattered electromagnetic field of each sandwich radome seam. Therefore, if the seams are distributed in a randomized way, in other words sandwich radome panels are designed such that the geometry of each panel is designed in a different type as given in Figure 42, constituted total scattered electromagnetic field with the vector summation of the scattered electromagnetic field of each panel seam will be with relatively small coefficients while compared with the relatively parallel distributed seam structured sandwich radome seams. Therefore, new side lobe level generations or increased side lobe levels can be prevented with this method.



Figure 42 – 18.9 Meter Diameter Sandwich Radome Panels and Panel Framework Geometry [3]

To express the importance of Geometrical Randomisation following simulation work is done in HFSS™. In this work, same number of seams is placed in front of the antenna at relatively same distance. The first design is very similar to the orange-peel type designed radome framework defined in Chapter 2. In this design, framework geometry is composed of parallel elements in azimuth and elevation. In the second design, the framework elements are placed in a totally randomized geometry to show the effect of Geometrical Randomization clearly. Figure 43 shows the design with orange-peel type radome framework structure.

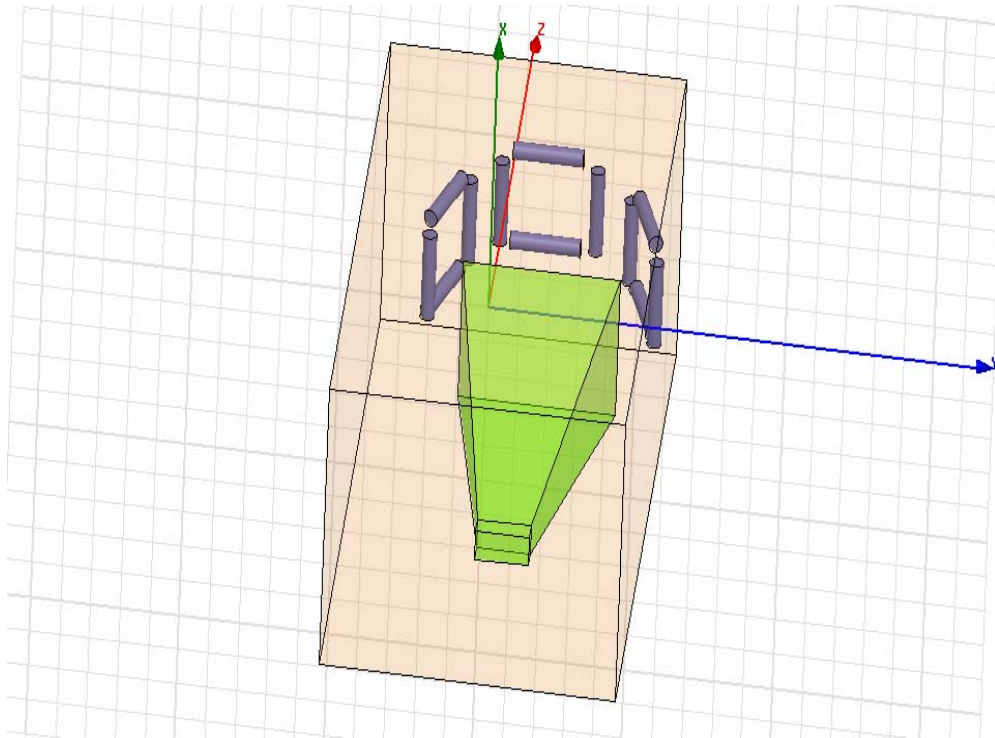


Figure 43 – Orange-Peel Radome Framework Design with  $2,8 \lambda$  Length and  $0,2 \lambda$  Diameter 12 Seams Placed at  $6\lambda$  Distance to the Antenna

Figure 44 shows the 3D polar plot of total far electromagnetic E-Field Pattern with orange-peel type designed sandwich radome seams in front of the antenna. As can be seen clearly from the figure, the pattern characteristics highly distorted with effect of cumulative scattering effect of each seam forming the framework. Shape of the main beam is highly distorted as presented. Moreover many new side lobes are generated with the effect of scattering.

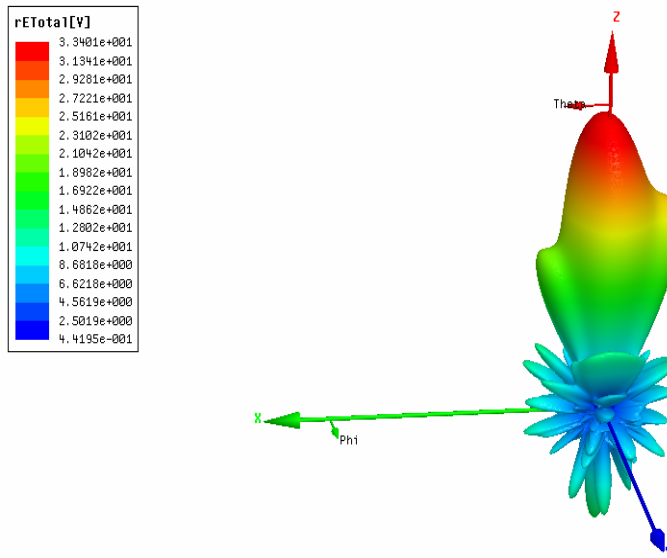


Figure 44 - 3D Polar Plot of Total E-Field Pattern of Orange-Peel Type Designed Sandwich Radome Framework with  $2.8 \lambda$  Length and  $0.2 \lambda$  Diameter 12 Seams Placed at  $6\lambda$  Distance to the Antenna

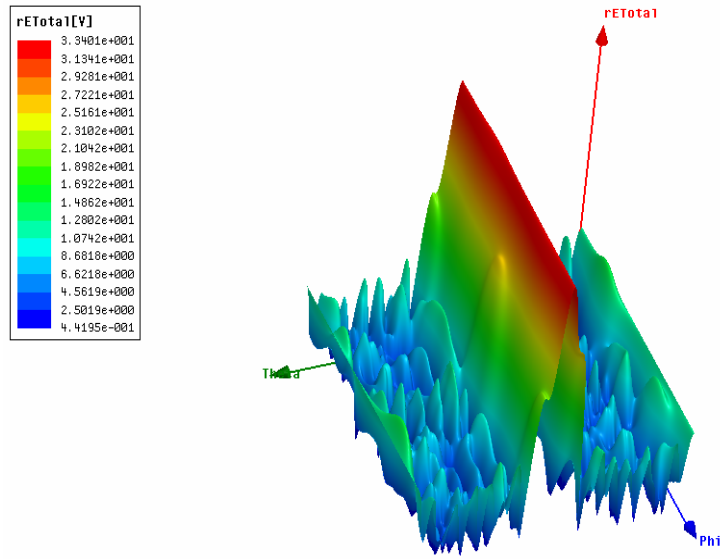


Figure 45 - 3D Rectangular Plot of the E-Field Pattern Characteristics of Orange-Peel Type Designed Sandwich Radome Framework with  $2.8 \lambda$  Length and  $0.2 \lambda$  Diameter 12 Seams Placed at  $6\lambda$  Distance to the Antenna

Figure 45 shows 3D Rectangular Plot of the Total E-Field Pattern of the orange-peel type designed Sandwich Radome framework in front of the antenna to clearly present the effect of cumulative scattering of each sandwich radome seam structure. The occurrence of high numbered side lobe levels and broadened main beam of the antenna is clearly presented in the figure.

After having the characteristics of parallel designed sandwich radome seam framework geometry, to show the importance of randomized distribution of sandwich radome seams following design is constructed in HFSS™ as given in Figure 46.

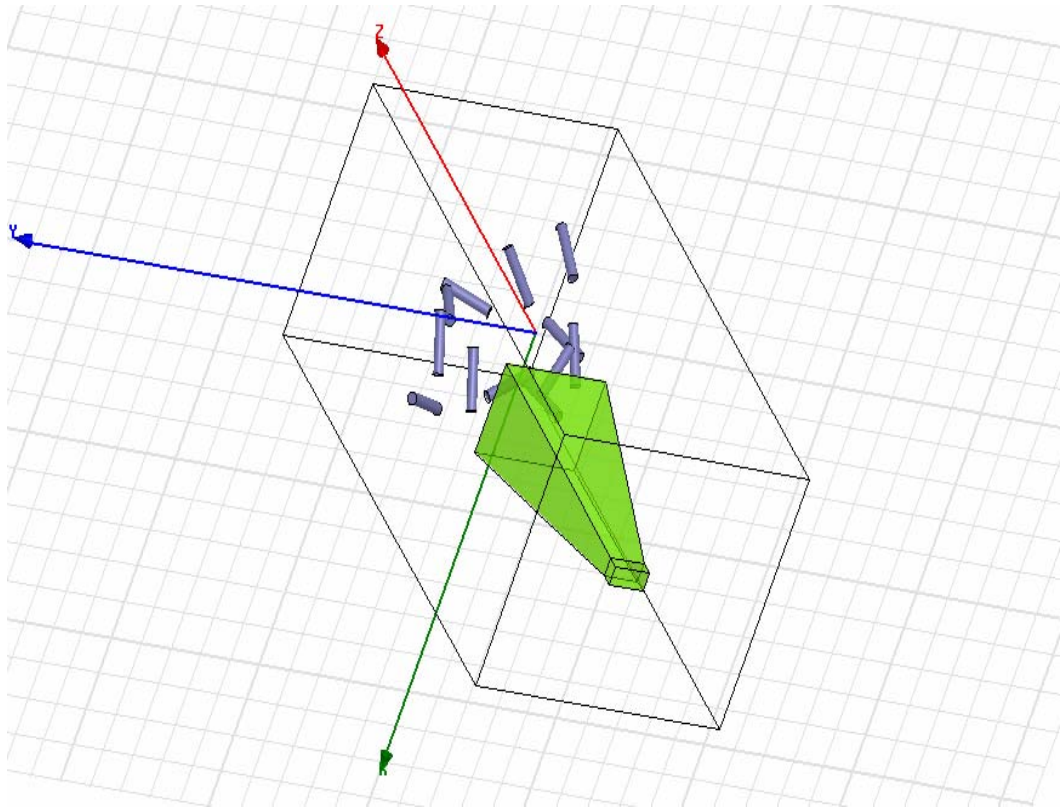


Figure 46 – Randomized Distribution of  $2,8 \lambda$  Length and  $0,2 \lambda$  Diameter 12 Seams Placed at Approximately  $6\lambda$  Distance In Front of the Antenna

Figure 47 shows the 3D Polar Plot of the total E-Field pattern characteristics of randomized distribution of seams in front of the antenna. When compared with the characteristics obtained with orange-peel type design in Figure 44, distortion of the antenna signal in Figure 47 with minimized cumulative scattering effect of each random distributed sandwich radome seam is quite less as expected. This figure shows the importance preventing parallel structures in the framework clearly.

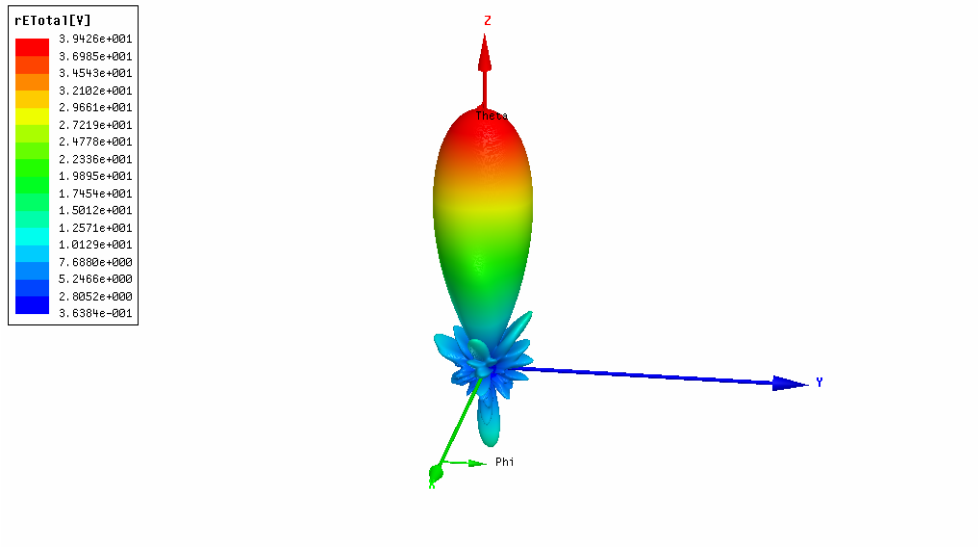


Figure 47 - 3D Polar E-Field Pattern of Random Distributed  $2,8 \lambda$  Length and  $0,2 \lambda$  Diameter 12 Seams Placed at Approximately  $6\lambda$  Distance In Front of the Antenna

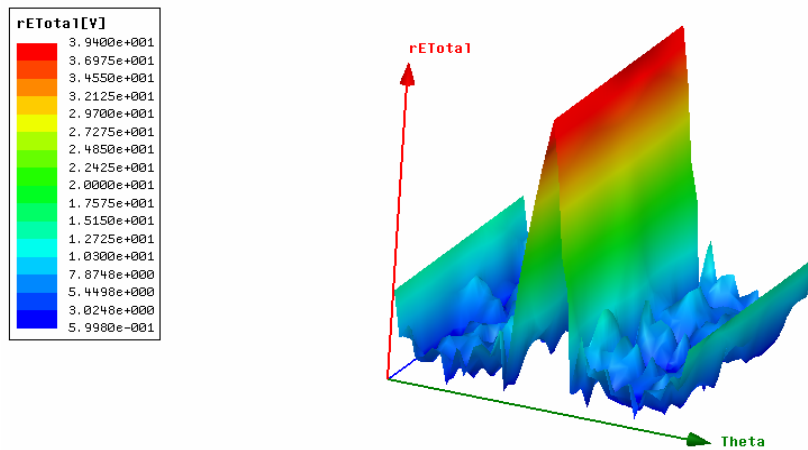


Figure 48- 3D Rectangular Total E-Field Pattern of Random Distributed  $2,8 \lambda$  Length and  $0,2 \lambda$  Diameter 12 Seams Placed at Approximately  $6\lambda$  Distance In Front of the Antenna

Figure 48 shows 3D Rectangular Plot of the Total E-Field Pattern of the Randomized Distribution of the Sandwich Radome Seams in front of the antenna. When compared with the characteristics in Figure 45, lower number of newly generated side lobes and sharper main beam are the important differences between two characteristics

#### **4.4 Electromagnetic Transparency Enhancement by Tuning the Seams in Sandwich Type Radomes**

In sandwich type radomes the framework materials are usually composed of dielectric materials such as polyamide foams, silicon dioxide, silicon nitrate etc. In these dielectric structures with the effect of incident antenna field, parallel and perpendicular polarization currents occur. These currents play the main role on the electromagnetic scattering effect of the framework structure of the sandwich type radomes. Enhancing electromagnetic transparency can be achieved if these polarization currents can be decreased. To decrease these polarization currents inside the framework structure of the sandwich radome, perfectly conducting materials are inserted inside the seam.

##### **4.4.1 Tuning the Seams in Sandwich Type Radomes**

It is known that perfectly conducting materials directly scatter the antenna incident electromagnetic signal such that IFR (induced field ratio) is -1. Therefore, even in the Metal Space Frame Radomes which are the most common radomes in the world, only the framework structure is composed conducting materials such as Aluminum. However in the Sandwich Radome case, the perfectly conducting materials are inserted in the dielectric framework to decrease high capacitance of the structure. It can be viewed as

inserting an inductor to the highly capacitive circuit to tune in. Inserting perfect electric conductors inside the radome seam is named as Tuning the Radome. Inserting these thin perfectly conducting materials inside the seams, decrease the polarization currents inside the framework structure. This degradation increases the electromagnetic transparency of the seams of the Sandwich Radome. With this design solution it is possible to design sandwich type radomes for antennas which operate at high frequencies.

#### **4.4.2 Effect of Tuning the Seams in Sandwich Type Radomes**

The effect of inserting perfect conductors inside the dielectric framework structure of the sandwich radome is emphasized by the following design in HFSS™. First, one horizontal dielectric cylinder which has a radius of 7 cm made of silicon dioxide (relative permittivity is 4 and relative permeability is 1) is inserted in front of the horn antenna near field at a distance of  $5\lambda$  distance from the horn as seen in the figure 49. In this simulation the radius of the dielectric seam is increased specifically to emphasize the tuning effect in the next step.



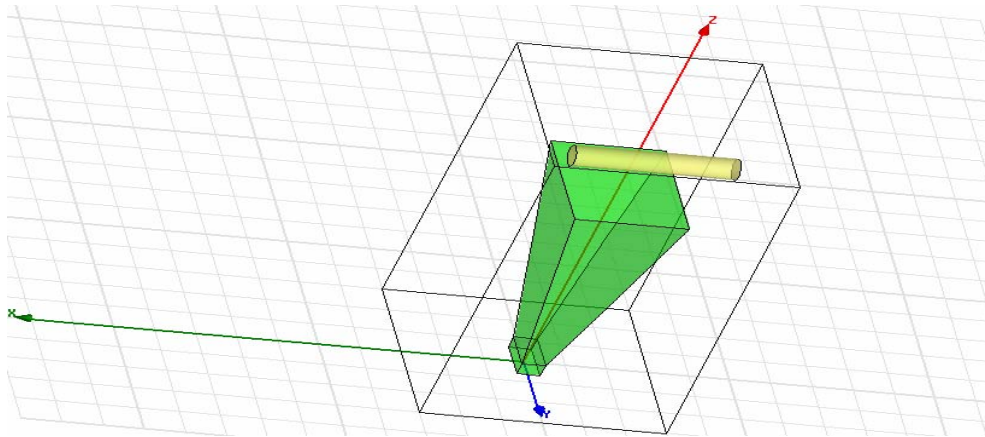


Figure 49 – Horizontal Silicon Dioxide Cylinder Seam with  $4,8 \lambda$  Length and  $0,47 \lambda$  Diameter Placed at  $5 \lambda$  Distance to the Horn Antenna

With this configuration following far electromagnetic E-field patterns obtained as given in Figures 50, 51 and 52.

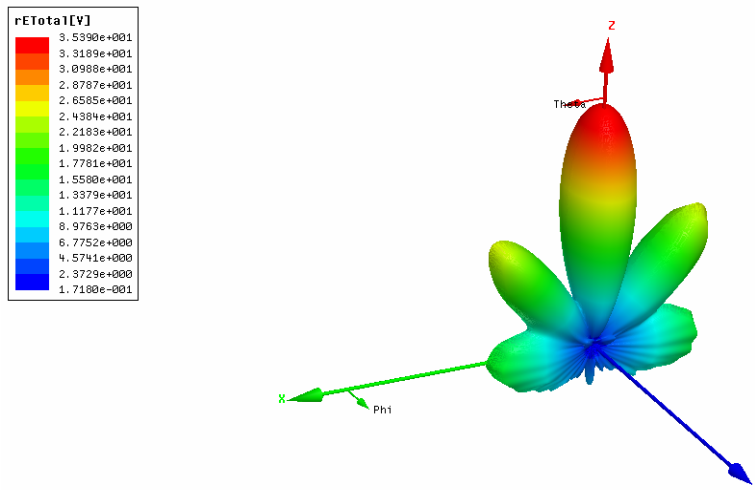


Figure 50 - 3D Polar Total E-Field of the Horizontal Silicon Dioxide Seam with  $4,8 \lambda$  Length and  $0,47 \lambda$  Diameter Placed at  $5 \lambda$  Distance to the Horn Antenna

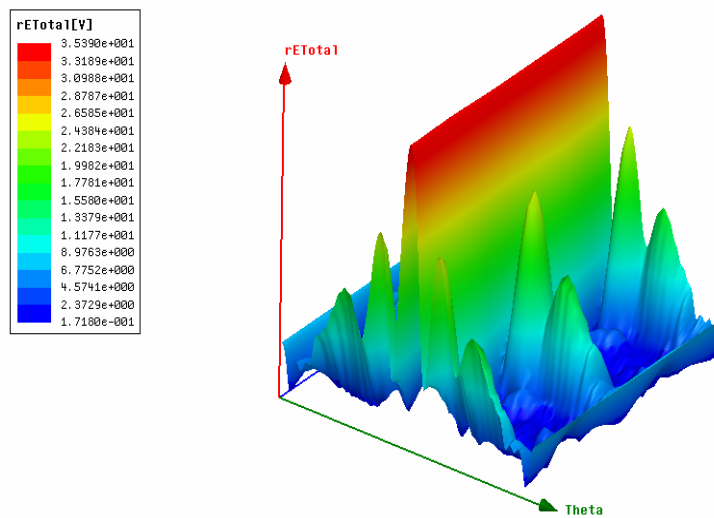


Figure 51 - 3D Rectangular Total E-Field of the Horizontal Silicon Dioxide Seam with  $4,8 \lambda$  Length and  $0,47 \lambda$  Diameter Placed at  $5 \lambda$  Distance to the Horn Antenna

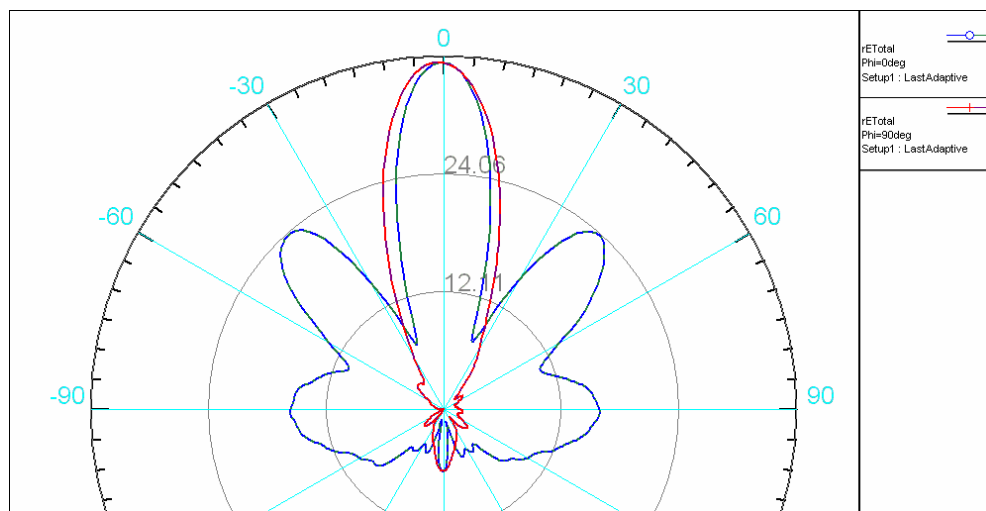


Figure 52 - 2D Total E-Field of the Horizontal Silicon Dioxide Seam with  $4,8 \lambda$  Length and  $0,47 \lambda$  Diameter Placed at  $5 \lambda$  Distance to the Horn Antenna

Figure 52 shows 2D total E-Field radiation characteristics of horizontal 7 cm radius silicon dioxide sandwich radome seam and the antenna. In this figure red line represents the E-plane ( $\phi = \pi / 2$ ) characteristics and blue line represents H-plane ( $\phi = 0$ ) characteristics of total E-Field.

Far field pattern characteristics show that the dielectric seam with 14 cm diameter has important effects on the total antenna far electromagnetic field characteristics. As can be observed easily from the 3D polar, rectangular plots and 2D plot of the system given in Figure 50, 51 and 52, there are two high valued side lobes formed with the angle of 45 and 90 degrees in elevation. The values of these side lobes are comparable to the main beam with the effect of increased radius of the seam structure. Therefore, this high scattering effect of the dielectric seam has to be decreased to have a high performance design.

An important solution to minimize this scattering effect in sandwich type radomes is Tuning the Seams. To show the effect of tuning on the electromagnetic transparency of this dielectric seam following design is done in HFSS™ as given in Figure 53. As seen in Figure 53 perfect electric conductors are inserted inside the same dielectric seam structure given in Figure 49.

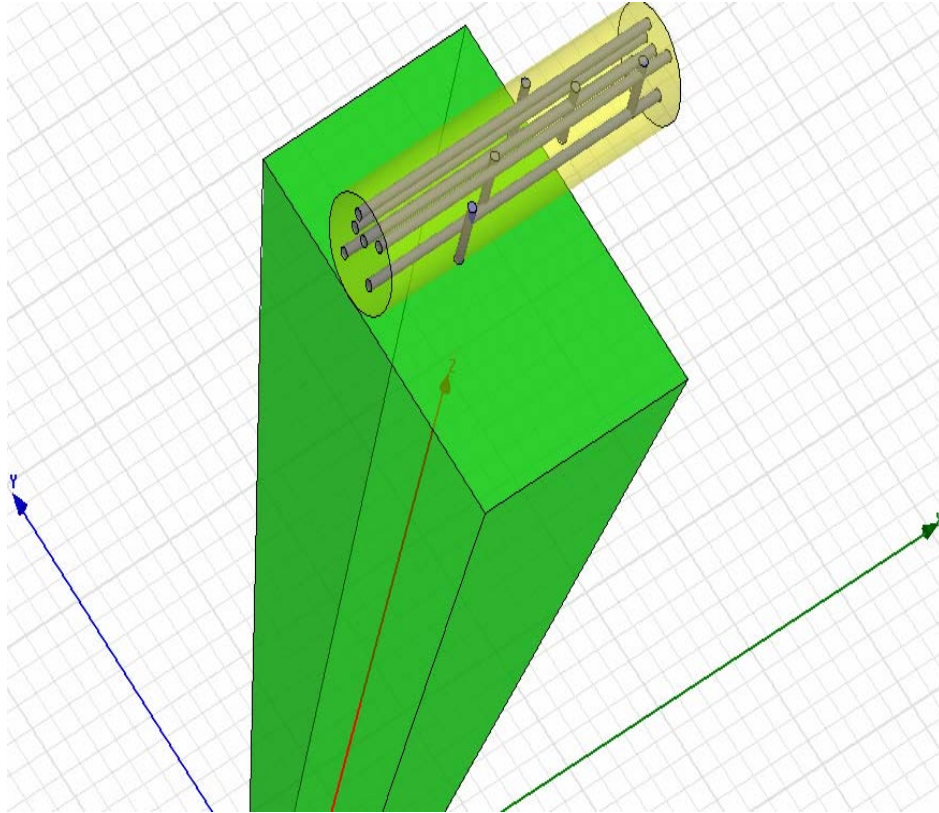


Figure 53 - Tuning Mechanism of the Silicon Dioxide Dielectric Seam with Perfect Electric Conductors

This modified seam is put at the same place as the pure dielectric one in Figure 49, so that the effect of tuning can be emphasized directly. With this tuned seam structure following far electromagnetic E-field pattern characteristics is obtained given in Figure 54, 55 and 56. Figure 54 and 55 represents 3D polar and rectangular plot of total E-Field radiation characteristics of tuned dielectric seam and the antenna. Figure 56 represents 2D total E-Field radiation characteristics of tuned dielectric seam and the antenna on the principal planes. In this figure red line represents the E-plane ( $\phi = \pi / 2$ ) characteristics and blue line represents H-plane ( $\phi = 0$ ) characteristics of total E-Field.

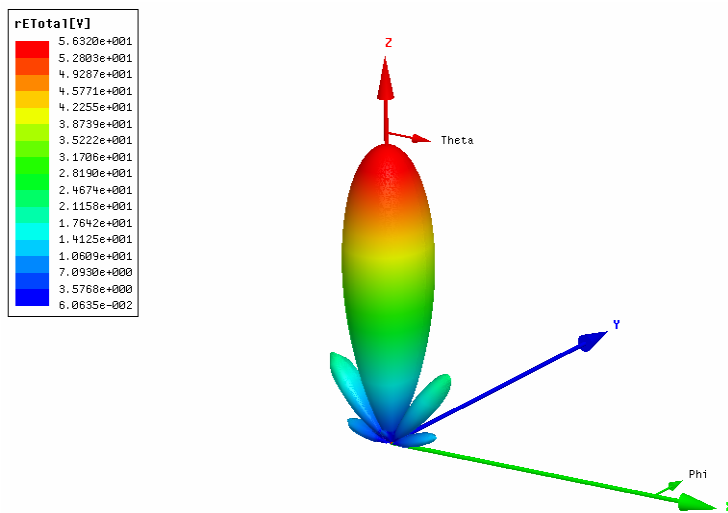


Figure 54 -3D Polar Plot of the Total E-Field Pattern of the Tuned Seam with  $4,8 \lambda$  Length and  $0,47 \lambda$  Diameter Placed at  $5 \lambda$  Distance to the Horn Antenna

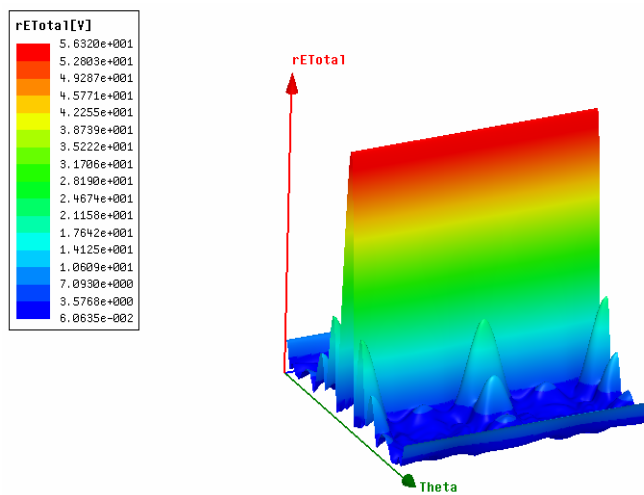


Figure 55 - 3D Rectangular Plot of the E-Field Pattern of the Tuned Seam with  $4,8 \lambda$  Length and  $0,47 \lambda$  Diameter Placed at  $5 \lambda$  Distance to the Horn Antenna

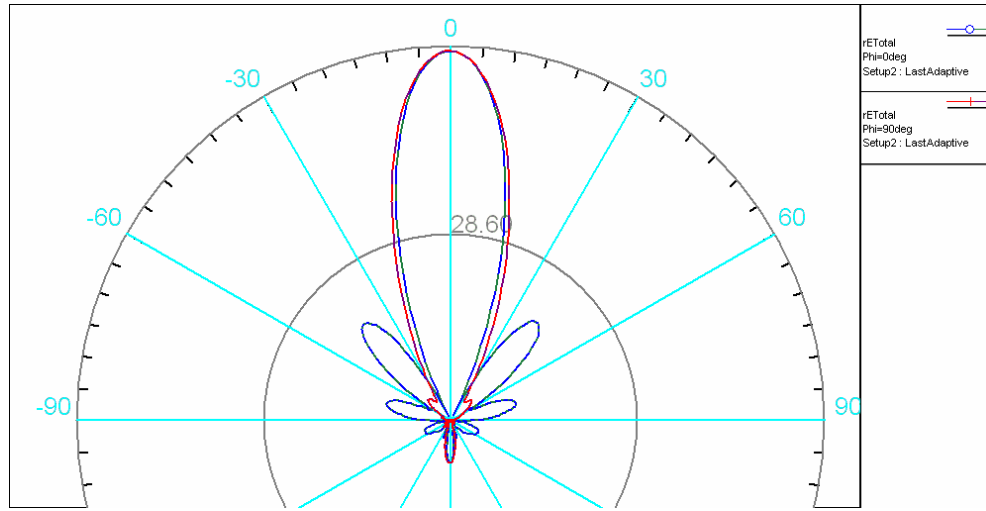


Figure 56 - 2D Total E-Field Radiation Characteristics of Tuned Sandwich Radome Seam with  $4.8 \lambda$  Length and  $0.47 \lambda$  Diameter Placed at  $5 \lambda$  Distance to the Horn Antenna

As expressed in far electromagnetic field pattern characteristics of tuned dielectric seam and the horn antenna, high side lobe levels at 45 degrees elevation are minimized while compared with the same characteristics of the pure dielectric seam. Side lobe level at 90 degrees elevation nearly disappeared which had been occurred with the effect of dielectric seam in front of the antenna. To sum up, inserting perfect electric conductors inside the framework structure of the sandwich radome enhances the electromagnetic transparency by degrading the scattering effect of the pure dielectric sandwich radome seam in the framework successively. This work shows the importance of tuning operation of the seams in high performance sandwich radome designs directly.

## **CHAPTER 5**

### **CONCLUSIONS**

Sandwich radomes are the best solution for high performance, discrete narrow band, large antenna systems to prevent them from harsh weather conditions, to maintain required operational performance of the system for long periods of time while having minimum effect on the electromagnetic fields transmitted and received by the inside antenna systems. When compared with other radome types investigated in this thesis, mechanical and electromagnetic features of sandwich radomes put forth importance of sandwich radome structures. Since sandwich radome panels are specifically manufactured considering operating frequency of the antenna and insulation need of environment, electromagnetic insertion loss is around 0.1 dB for typical applications. However, transmission loss due to the framework of the sandwich radome panels is around 0.4 dB up to 10 dB for a design which only the constructional requirements are considered. Therefore, electromagnetic analysis and enhancing electromagnetic transparency of the framework structure of the sandwich radomes are very crucial for high performance designs.

In this thesis, after the investigation of most common radome types Sandwich Radomes are presented with their detailed features including structural and electromagnetic properties. Electromagnetic scattering

analysis of the Sandwich Radome framework is done. In this analysis, as a first step, scattering analysis of one dielectric cylinder seam is done. In the analysis, pyramidal horn type antenna is used because of the well known information on the near electromagnetic fields of the antenna. In fact the analysis is applicable to all antenna systems with the knowledge of antenna near electromagnetic field formulations. In the next step the analysis done for one seam structure is generalized for arbitrary numbered distributed seams with different angles with respect to the antenna. As a final step, total far electromagnetic fields of the horn antenna and total electromagnetic scattered fields by the framework structure of Sandwich Radomes are combined to express the total antenna system far electromagnetic fields. Finally, using Ansoft HFSS<sup>TM</sup> program electromagnetic field patterns of antenna and framework structure of Sandwich Radomes are simulated with various antenna and seam distributions. This analysis is done with pyramidal horn type antenna as a case study which has a resonant frequency of 1 GHz with the dimensions 76.2 cm ( $2.54\lambda$ ) and 55.9 cm ( $1.86\lambda$ ) at the aperture, funnel length of 157.4 cm ( $5.24\lambda$ ) with base of the horn dimensions of 9.05 cm ( $0.3\lambda$ ), 11.4 cm ( $0.38\lambda$ ) and 25.86 cm ( $0.862\lambda$ ) at this resonant frequency. Seams are put at different angles and with different polarizations with respect to the aperture of the antenna to generalize the scattering effect of the seam structures on the antenna far electromagnetic field patterns. Numerical experiment is repeated for the cases of various number of seams in front of the antenna. Obtained results show the success of electromagnetic scattering analysis.

In this thesis, there are two important design solutions suggested to enhance electromagnetic transparency of the radome framework of the Sandwich Radomes. The solutions are named as Geometrical Randomization and Tuning the Seams. In Ansoft HFSS<sup>TM</sup>, the effects of two design solutions are expressed successively.



To show the importance of Geometrical Randomization, same length and same number of seams are distributed randomly around the antenna at the resonant frequency of 1 GHz in Ansoft HFSS™ design program. Then the total scattering effect is compared with parallel distributed radome seam structures as in the Orange-Peel Sandwich Radome Type around the same antenna at the same frequency. The result shows that electromagnetic transparency of radome seams is enhanced via increasing randomness distribution of the seams as suggested. Simulations show that total scattering effect of orange-peel type geometric distribution of seams is higher than the randomized geometrical distribution of same number of seams. Furthermore, structural investigation of orange-peel type geometry and quasi-random type geometry of sandwich type radomes has shown that quasi-random geometric distribution of the framework strengthens the structure more than the orange-peel type geometric distribution of seams in the framework. It should be kept mind that, while increasing the randomness of the seams in quasi-random geometry it is important to keep total seam length as low as possible. Because, if total seam length increase is not controlled, it causes higher transmission loss due to the framework and this will become an unwanted drawback. Moreover, it should always be considered that producing and installing costs of the sandwich radome panels increase by increasing randomness of the panels.

In this thesis work, a second solution for enhancing the transparency of sandwich radomes is expressed and named as Tuning the Seams. This solution broadens the usage of sandwich type radomes up to high frequencies because of the minimization of the framework scattering fields of the sandwich radomes. In this method perfect electric conductors are inserted inside the seam structure. This composite structure enhances the transparency of the framework because of the degradation of the polarization currents inside the seam structure. Its effect on the scattering

field of the framework is shown via Ansoft HFSS™ simulations successively.

As a future work, electromagnetic responses of different composite materials constituting the sandwich radome panels and the panel framework can be investigated. Finding the best frequency band of operation information for different sandwich radome materials including the framework and the panel structures will increase the importance of the investigation. Moreover, as a future work insertion loss due to the panels and the framework structure which is composed of dielectric and conducting materials can be added to the scattering analysis in this thesis work. Insertion loss occurrence by tuning the seams with conducting materials can be investigated with this future work. Furthermore, investigation on the mechanical properties including critical buckling speed and the safety factor can be done for different sandwich radome materials for the framework and the panels. Finally, all the investigations may be combined with cost analysis of the materials constituting the sandwich radome structure itself and the building operation difficulty with these specific materials put forth economic and constructional manufacturability of the designs with Sandwich Radomes.

## REFERENCES

- [1] Wikipedia, “Radome”, <http://en.wikipedia.org/wiki/Radome>, January 18<sup>th</sup> 2009, Last date accessed: March 2009
- [2] Antennas For Communications, <http://www.radome.net>, January 18<sup>th</sup> 2009, Last date accessed: March 2009
- [3] Essco Radomes, <http://www.esscoradomes.com>, January 18<sup>th</sup> 2009, Last date accessed: March 2009
- [4] Micris Radomes, <http://www.micris.co.uk/radomes.php>, January 25<sup>th</sup> 2009, Last date accessed: March 2009
- [5] Radome Panel Transportation Preparation, [http://www.thecoolroom.org/news/RadomePieces\\_Crate.jpg](http://www.thecoolroom.org/news/RadomePieces_Crate.jpg), January 25<sup>th</sup> 2009, Last date accessed: March 2009
- [6] Radome Panel Installation, <http://www.radomes.com>, January 25<sup>th</sup> 2009, Last date accessed: March 2009
- [7] Wikipedia, “Insertion Loss”, [http://en.wikipedia.org/wiki/Insertion\\_loss](http://en.wikipedia.org/wiki/Insertion_loss), January 25<sup>th</sup> 2009, Last date accessed: March 2009
- [8] W.T.Rusch, J.A.Hansen, R.Mitra, C.A.Klein, “Forward scattering from square cylinders in the resonance region with application to aperture blockage.” IEEE Trans. Antenna Propaga.vol AP-24, no.2 pp-182-189, Mar. 1976

[9]EsscoRadomes,<http://www.l3com.com/essco/resources/ifrdefinition.html>, January 26 th 2009, Last date accessed: March 2009

[10] Essco Radomes, Hydrophobic Coating,  
<http://www.l3com.com/essco/resources/hydrophobiccoating.html>, January 26 th 2009, Last date accessed: March 2009

[11] Saint - Gobain Performance Plastics “Radome Installations\_polyester”  
Aselsan Inc. Proposal 162-1561 D May 2004

[12] Reuven Shavit, Adam P.Smolski, Eric Michielssen and Raj Mittra  
“Scattering Analysis of High Performance Large Sandwich Radomes” IEEE  
Transaction on Antennas and Propagation, Vol.40, No.2 February 1992

[13] Saint-Gobain Flight Structures, “Sandwich Radome Types” ,  
<http://www.radome.com>, January 31 th 2009, Last date accessed: March 2009

[14] V.J. Dicaudo “Determining Optimum C-Sandwich Radome Thickness  
by Means of Smith Chart”, IEEE Transections on Antennas and  
Propagation, pp 822-823, November 1967

[15] I. D. King “Application of On-Surface Radiation Condition to  
Electromagnetic Scattering by Conducting Strip”, IEEE Electronic Letters  
Vol.25 No.1 5<sup>th</sup> January 1989

[16] Doris I. WU, Motohisa Kanda, “Comparison of Theoretical and  
Experimental Data for the Near Field of an Open-Ended Rectangular  
Waveguide” IEEE Transactions on Electromagnetic Compatibility, Vol.31  
No.4. November 1989

[17] R.E.Collin, “Antennas and Radiowave Propagation”, McGraw-Hill  
International Editions 3<sup>rd</sup> printing 1988.

[18] George T. Ruck, Donald E. Barrick, William D. Stuart, Clarence K. Krichbaum, "Radar Cross Section Handbook", Plenum Press New York 1970.

[19] Plamen I. Dankov, Vesselin N. Peshlov, Mario Gachev, "Modeling and Characterization of Multilayer Antenna Radomes with Anisotropic Materials", University of Sofia St. Kliment Ohridsky

## APPENDIX

### Horn Antenna Far Electromagnetic Fields

Far electromagnetic fields of the horn antenna are determined from the aperture electromagnetic fields.

The dominant mode of the horn antenna is  $TE_{10}$  mode. Let's define the antenna aperture dimensions as "a" and "b" relatively. Then the typical aperture fields are defined as:

$$\vec{E} = E_0 \cos\left(\frac{\pi x}{a}\right) e^{-j\beta z} \hat{a}_y \quad (1)$$

$$\vec{H} = -E_0 Y_0 \cos\left(\frac{\pi x}{a}\right) e^{-j\beta z} \hat{a}_x \quad (2)$$

where

$$\beta = \sqrt{k_o^2 - \left(\frac{\pi}{a}\right)^2} \quad (3)$$

$$\vec{f}(x, y) = \int_{-b/2}^{b/2} \int_{-a/2}^{a/2} \vec{E}_a e^{jk_x x} e^{jk_y y} dx dy \quad (4)$$

where  $\vec{E}_a$  is the aperture E-Field

Then,

$$E_{\theta} = \frac{jk_0}{2\pi r} e^{-jk_0 r} (f_x \cos \phi + f_y \sin \phi) \quad (5)$$

$$E_{\phi} = \frac{jk_0 \cos \theta}{2\pi r} e^{-jk_0 r} (f_y \cos \phi - f_x \sin \phi) \quad (6)$$

$$f_x = 0 \quad \text{since} \quad \overrightarrow{E_x} = 0 \quad (7)$$

$$f_y = \int_{-b/2}^{b/2} \int_{-a/2}^{a/2} E_0 \cos\left(\frac{\pi x}{a}\right) e^{-jk_x x} e^{-jk_y y} dx dy \quad (8)$$

$$f_y = 2\pi ab E_0 \frac{\sin[k_y(b/2)]}{k_y(b/2)} \frac{\cos[k_x(a/2)]}{\pi^2 - [k_x(a/2)]^2} \quad (9)$$

where,

$$k_x = k_0 \sin \theta \cos \phi \quad (10)$$

$$k_y = k_0 \sin \theta \sin \phi \quad (11)$$

$$\begin{aligned}
\overrightarrow{E_{ANTENNA}} = & \frac{jk_0}{r} E_0 a b e^{-jk_0 r} \left[ \sin \phi \frac{\sin(k_0 \sin \theta \sin \phi \frac{b}{2})}{k_0 \sin \theta \sin \phi \frac{b}{2}} \right] \left\{ \right. \\
& \left[ \frac{\cos(k_0 \sin \theta \cos \phi \frac{a}{2})}{\pi^2 - 4(k_0 \sin \theta \cos \phi \frac{a}{2})^2} \right] \widehat{a}_\theta \\
& + \left( \cos \theta \cos \phi \frac{\sin(k_0 \sin \theta \sin \phi \frac{b}{2})}{k_0 \sin \theta \sin \phi \frac{b}{2}} \right) \left[ \frac{\cos(k_0 \sin \theta \cos \phi \frac{a}{2})}{\pi^2 - 4(k_0 \sin \theta \cos \phi \frac{a}{2})^2} \right] \widehat{a}_\phi \left. \right\} \\
& (12)
\end{aligned}$$